Exact Solution of Kinetic Analysis for Thermally Activated Delayed Fluorescence Materials

Journal:	*The Journal of Physical Chemistry*
Manuscript ID	jp-2021-04056x.R2
Manuscript Type:	Article
Date Submitted by the Author:	n/a

Complete List of Authors:	Tsuchiya, Youichi; Kyushu University , OPERA Diesing, Stefan; University of St Andrews Bencheikh, Fatima ; Kyushu University, Center for Organic Photonics and Electronics Research (OPERA) wada, yoshimasa; The University of Tokyo, Institute of Industrial Science dos Santos, Paloma Laís ; University of St Andrews Kaji, Hironori; Kyoto University, Institute for Chemical Research Zysman-Colman, Eli; University of St Andrews, Chemistry Samuel, Ifor D. W.; University of St Andrews Adachi, Chihaya; Kyushu University, Center for Organic Photonics and Electronics Research (OPERA)

Exact solution of kinetic analysis for thermally activated delayed fluorescence materials

Youichi Tsuchiya [a*], Stefan Diesing [b,c], Fatima Bencheikh [a], Yoshimasa Wada [d], Paloma L. dos Santos [c], Hironori Kaji [d], Eli Zysman-Colman [b*], Ifor D. W. Samuel [c*], and Chihaya Adachi [a,e*]

[a] *Center for Organic Photonics and Electronics Research (OPERA), Kyushu University, 744, Motooka, Nishi-ku, Fukuoka 819-0395, Japan*

[b] *Organic Semiconductor Centre, EaStCHEM School of Chemistry, University of St Andrews, St Andrews, Fife, KY16 9ST, UK*

[c] *Organic Semiconductor Centre, SUPA School of Physics and Astronomy, University of St Andrews, St Andrews, Fife, KY16 9ST, UK*

[d] *Institute for Chemical Research, Kyoto University, Uji, Kyoto, 611-0011, Japan*

[e] *International Institute for Carbon Neutral Energy Research (WPI-I^{2}CNER), Kyushu University, 744, Motooka, Nishi-ku, Fukuoka 819-0395, Japan*

*Email: tsuchiya@opera.kyushu-u.ac.jp, eli_journals@zysman-colman.com, idws@st-andrews.ac.uk, adachi@cstf.kyushu-u.ac.jp

ABSTRACT: The photophysical analysis of thermally activated delayed fluorescence (TADF) materials has become instrumental to providing insight into their stability and performance, which is not only relevant for organic light-emitting diodes (OLED), but also for other applications such as sensing, imaging and photocatalysis. Thus, a deeper understanding of the photophysics underpinning the TADF mechanism is required to push materials design further. Previously reported analyses in the literature of the kinetics of the various processes occurring in a TADF material rely on several *a priori* assumptions to estimate the rate constants for forward and reverse intersystem crossing (ISC and RISC, respectively). In this report, we demonstrate a method to determine these rate constants using a three-state model together with a steady-state approximation and, importantly, no additional assumptions. Further, we derive the exact rate equations, greatly facilitating a comparison of the TADF properties of structurally diverse emitters and providing a comprehensive understanding of the photophysics of these systems.

INTRODUCTION

In recent years, organic thermally activated delayed fluorescence (TADF) materials have attracted significant attention within the organic semiconductor community as TADF provides a route for 100% internal quantum efficiency in organic light-emitting diodes (OLEDs), without the need to use precious noble metal complexes.[1-4] Distinct from phosphors that rely on large spin-orbit coupling to drive the conversion of singlet excitons to triplets and then phosphorescence of the latter, organic TADF materials convert triplet excitons to singlet excitons by taking advantage of the small energy gap (ΔE_{ST}), typically taken as less than 200 meV, between the lowest singlet (S_1) and triplet (T_1) excited states. As T_1 excitons are efficiently upconverted into an S_1 level through a reverse intersystem crossing (RISC) route, OLEDs can harvest the 75% of electrically generated excitons that are triplets for electroluminescence (EL) as delayed fluorescence from the singlet excited state. The most common molecular design that shows small ΔE_{ST} is based on a donor-acceptor architecture wherein there is poor electronic communication between the two moieties, resulting in a small

exchange integral and a correspondingly small ΔE_{ST}. TADF materials typically exhibit dual fluorescence consisting of a prompt nanosecond fluorescence originating from the radiative decay of directly formed singlet excitons and a microsecond to millisecond delayed fluorescence that originates from the multiple ISC and RISC cycles preceding emission from the singlet excited state. The performance of the OLED, and in particular the efficiency roll-off and the device stability, are intimately linked to the population of the long-lived triplet excitons. As RISC is the slowest process typically observed in OLEDs using organic TADF emitters, the optimization of the device performance is intimately linked to increasing the rate constant associated with RISC, k_{RISC}. Thus, it is essential to have an accurate measure of this key rate constant.

Many researchers have tried to understand the photophysics of TADF materials by curve fitting the time-resolved photoluminescence (PL) decays using a conventional rate equation strategy that accounts for each decay process. While this approach is useful, most previous analyses require several *a priori* assumptions, leading to rather large deviations from experiment or, in some cases, completely incorrect conclusions. For example, in 1983, McMillin and co-workers explained the TADF behavior of a Cu(I) complex using a Boltzmann statistical analysis of the population equilibrium of excitons in the S_1 and T_1 states, this analysis based on several assumptions. These included that the intersystem crossing (ISC) efficiency (Φ_{ISC}) is almost unity and the rate constant of nonradiative decay from the singlet excited state (k_{nr}^S) is 0.[5] In a very early study in 2012, our group applied this method to organic TADF materials having nearly 100% PL quantum yield (PLQY).[6] Here, k_{TADF} was given by

$$k_{TADF} = \frac{1}{3} k_r^S \exp\left(\frac{-\Delta E_{ST}}{RT}\right), \quad (1)$$

where k_{TADF} is a triplet decay rate via S_1 including ISC/RISC cycles (not the element value of k_{RISC}), R and T are the ideal gas constant and the temperature, respectively. However, the materials that can be analyzed using this method are quite limited because of the demanding assumptions this model makes. Subsequently, in our first kinetics analysis model in 2012, k_{RISC} was obtained but with a less stringent set of assumptions that the radiative and nonradiative decay rate constant from a singlet excited state (k_r^S) and k_{nr}^S, respectively, and the ISC rate constant (k_{ISC}) are all significantly larger than both the rate constants of nonradiative decay from a triplet excited state (k_{nr}^T) and k_{RISC}; further, it was assumed that radiative decay from a triplet excited state (k_r^T) does not occur.[7] In our second, revised, kinetics analysis study, we further simplified the model by imposing the additional assumption that $k_{nr}^S = 0$,[8] which implies that k_r^S and k_{ISC} are significantly larger than k_{nr}^S and k_{RISC}. Within this framework, k_{ISC} and k_{RISC} can be formulated as:

$$k_{RISC} = \frac{k_p k_d}{k_{ISC}} \cdot \frac{\Phi_{DE}}{\Phi_{PF}}, \quad (2)$$

$$k_{ISC} = k_p(1 - \Phi_{PF}), \quad (3)$$

where Φ_{PF}, Φ_{DE}, k_p and k_d are the experimentally obtained PL efficiencies and decay rates for the prompt and delayed emissions. In 2015, Kaji and co-workers carefully explained to derive k_{RISC} when ΔE_{ST} is quite small.[9] In 2016, Wu, Wong and co-workers arrived at the same equations as those of Eqs. 2 and 3, but by imposing fewer assumptions in their model.[10] In the same paper, they also obtained the following equation with the assumption of $k_r^T = k_{nr}^T = 0$ as:

$$k_{RISC} = \frac{k_p k_d}{k_r^S} \Phi_{PLQY}, \quad (4)$$

Dias, Penfold and Monkman more recently proposed a model that applies for TADF emitters that show a large fraction of delayed emission, i.e., $\Phi_{DE}/\Phi_{PF} > 4$, and with the assumptions that $k_r^T = k_{nr}^T = 0$.[11]

$$k_{RISC} = k_d \frac{\Phi_{PF} + \Phi_{DE}}{\Phi_{PF}}, \quad (5)$$

Kaji and co-workers removed the constraint that $\Phi_{DE}/\Phi_{PF} > 4$ and showed that k_{RISC} could be estimated with only the assumptions that $k_r^T = k_{nr}^T = 0$.[12]

$$k_{RISC} = \frac{k_p + k_d}{2} - \sqrt{\left(\frac{k_p + k_d}{2}\right)^2 - k_p k_d \left(1 + \frac{\Phi_{DE}}{\Phi_{PF}}\right)}. \quad (6)$$

Taking each a different approach, Hasse, Brütting, Monkman and co-workers demonstrated the direct fitting of the time-resolved PL decays using the rate constants as fitting parameters,[13] while Nguyen *et al.* provided an analysis model derived from experiments employing an exciton quencher.[14] Goodson and co-workers extracted the triplet decay rate using transient absorption (TA) measurement as a proxy for the RISC rate constant, but they did not appear to consider cycling between the singlets and triplets.[15] The constraints and assumptions for these RISC rate constant estimations are summarized in Table S1. Since there are now a large number of different models used to estimate k_{RISC}, each with their own set of assumptions, it has become impossible to accurately compare the estimated rate constants across these studies, complicating any meta-analysis. To reduce the number of assumptions and the differences in estimated k_{RISC}, Φ_{ISC} must be measured experimentally.

Because Φ_{ISC} and its related rate constant k_{ISC} are two of the essential parameters of photochemical processes that implicate triplet states, dating back to before 1970, several groups have focused on an estimation method of accurate Φ_{ISC}. Scott and Maltenieks proposed a method to estimate k_{ISC} using triplet absorption under steady-state conditions.[16] To apply this method to TADF materials, their equation can be rewritten as

$$\Phi_{ISC} = \frac{\rho(\lambda)_{SS} k_d}{\varepsilon_T(\lambda) I_a l}, \quad (7)$$

where $\rho(\lambda)_{SS}$ is the optical density change due to the triplet-triplet absorption from a T_1 state to a higher-lying triplet (T_n) state at the steady-state condition, $\varepsilon_T(\lambda)$ is the triplet-triplet extinction coefficient, I_a is the rate of absorption of exciting light, and l is the optical path length. It should be noted that $\varepsilon_T(\lambda)$ can be estimated experimentally.[17] In another study, Berberan-Santos *et al.* provided an estimation of Φ_{ISC} by fitting the intensity ratio of the prompt and delayed emission (I_{PF}/I_{DF}), corresponding to Φ_{PL}^p/Φ_{PL}^d, vs $1/T$ by using Eq. 8.[18]

$$\ln\left[\frac{I_{PF}}{I_{DF}} - \left(\frac{1}{\Phi_{ISC}} - 1\right)\right] = \frac{\Delta E_{ST}}{R} \cdot \frac{1}{T} + \ln\left(\frac{k_r^T + k_{nr}^T}{\bar{k}_{RISC}}\right), \quad (8)$$

where $\bar{k}_{RISC}$ is the average rate constant for RISC. The shape of the plot is very sensitive to Φ_{ISC}, and is normally not linear. Continuous variation of Φ_{ISC} within the search for maximum linearity yields its best value. It should be noted that this method assumes that $(k_r^T + k_{nr}^T)$ and Φ_{ISC} are each essentially temperature independent. They also provided another analysis method for Φ_{ISC}, shown in Eq. 9, which combines a steady-state condition and a time-resolved analysis.[19]

$$\tau_{DF} = \tau_{Phos}^0 - \left(\frac{1}{\Phi_{ISC}} - 1\right)\tau_{Phos}^0 \frac{I_{DF}}{I_{PF}}, \quad (9)$$

where τ_{DF} is the delayed fluorescence lifetime $(1/k_d)$ and τ_{Phos}^0 is the low-temperature phosphorescence lifetime without any contribution to the emission associated with TADF, which means $1/(k_r^T + k_{nr}^T)$. This method also assumes that $(k_r^T + k_{nr}^T)$ is temperature independent. Our group demonstrated an estimation of Φ_{ISC} for thin film samples by combining pulse-excited electroluminescence (EL) and PL measurements.[7] Here, Φ_{ISC} can be obtained as

$$\Phi_{ISC} = \frac{3N}{M - N}, \quad (1.10)$$

where M and N are the quantum yield ratio of delayed fluorescence and prompt fluorescence for EL and PL, respectively; $\Phi_{EL}^d/\Phi_{EL}^p = M$, $\Phi_{PL}^d/\Phi_{PL}^p = N$. This method is very effective since it requires only the ratio of initial exciton distribution between S_1 and T_1 states, although this model is only relevant for thin films where OLED driving is applicable. Very recently, Naito *et al.* reconsidered the estimation method to obtain k_{ISC} from PL decay measurements under the assumption of $k_r^S + k_{ISC} \gg k_{RISC} \gg k_r^T + k_{nr}^T$, (Eq. 11).[20] This is a reasonable assumption for efficient organic TADF emitters.

$$\Phi_{ISC} = \frac{\Phi_{DF} + \Phi_{Phos}}{\Phi_r^S + \Phi_{DF} + \Phi_{Phos}} = \frac{\Phi_{DE}}{\Phi_{PLQY}}. \quad (11)$$

This equation for Φ_{ISC} converges to our three-state analysis (see Eq. S6.4) when $\Phi_{nr}^T = 0$ and $\Phi_r^T = 0$ are employed; however, we note that Eq. 11 is derived without these assumptions. This method should only be applied at around room temperature for organic TADF materials where triplet excitons mainly decay by a RISC path. Naito *et al.* also provided an equation for Φ_{ISC} determined at low temperature where the TADF is completely suppressed. For the temperature region where contributions from nonradiative decay paths cannot be ignored, an alternative approach using the temperature dependence of the prompt fluorescence rate is also provided.

Thus, if thin film samples are available, our model using Eq. 10 is the most promising and provides the most accurate determination of Φ_{ISC}. Without considering the complexity of the experimental setup and the associated specialized instrumentation, the method proposed by Scott and Malteniekes should be employed for solution-state samples. Both methods provided by Berberan-Santos *et al.* assume that $(k_r^T + k_{nr}^T)$ is temperature independent, which is a limitation of their methods as k_{nr}^T usually possesses a temperature dependence that is explained in terms of the thermal quench model.[21,22] The method of Naito *et al.* should be useful as it does not assume temperature independence for $(k_r^T + k_{nr}^T)$; however, it cannot be applied to inefficient TADF materials.

As explained above, most of the previously reported rate equations used for TADF compounds are based on models derived from highly emissive materials and assume $\Phi_{nr}^S = 0$ or $\Phi_{nr}^T = 0$, in order to obtain an estimation of Φ_{ISC}. Therefore, most of these previously reported rate equations are not appropriate for the analysis of low efficiency TADF materials. However, we often find reports that uncritically employ these models and equations to extract rate constants for low efficiency materials. In addition, assumptions such as $\Phi_{nr}^S = 0$ or $\Phi_{nr}^T = 0$ raise the question about "which parameter should be set to zero". Here, we introduce two kinetics analysis methods for TADF materials based on a three-state system of S_0, S_1, and T_1. In our first method where we invoke a steady-state approximation, no other assumptions are required in order to derive the set of rate constants related to the emission of TADF materials. This method not only can help in our understanding of TADF processes, but it can demonstrate the connections between several previously reported methods; however, this method still has the weakness in terms of providing an accurate estimation of Φ_{ISC}. To resolve this outstanding issue, we then present a derived exact solution to provide precise rate constants in the kinetics analysis of TADF materials.

RESULT AND DISCUSSION

Exact equation for emission decay curve for a three-state system. We first present an exact equation to model the emission decay that occurs from a three-state system comprising S_1 and T_1 coupled excited states and the S_0 ground state (Figure 1). The combined decay rates from both excited states in the absence of exciton-formation processes can be formulated as

$$\frac{d[S_1]}{dt} = -(k_r^S + k_{nr}^S + k_{ISC})[S_1] + k_{RISC}[T_1], \quad (12)$$

$$\frac{d[T_1]}{dt} = -(k_r^T + k_{nr}^T + k_{RISC})[T_1] + k_{ISC}[S_1], \quad (13)$$

where $[S_1]$ and $[T_1]$ are the populations of S_1 and T_1 excitons. The differential equations, Eqs. 12 and 13, are a system of ordinary differential equations of the general formula of $d\vec{Y}(t)/dt = A\vec{Y}(t)$, and can be written as,

$$\frac{d}{dt}\begin{pmatrix}[S_1]\\ [T_1]\end{pmatrix} = \begin{pmatrix}-k^S & k_{RISC}\\ k_{ISC} & -k^T\end{pmatrix}\begin{pmatrix}[S_1]\\ [T_1]\end{pmatrix}, \quad (14)$$

where $k^S = k_r^S + k_{nr}^S + k_{ISC}$ and $k^T = k_r^T + k_{nr}^T + k_{RISC}$, respectively. The general solution to this system is given by,

$$\vec{Y}(t) = \sum_{i=1}^{n} c_i \vec{v_i} \exp(\lambda_i t), \quad (15)$$

where $\vec{v_i}$ is the eigenvector with corresponding eigenvalue λ_i of the matrix A, and c_i is a constant depending on the initial conditions. For the matrix A in Eq. 14, the eigenvalues can be calculated as,

$$\det(A - \lambda E) = \det\left[\begin{pmatrix}-k^S - \lambda & k_{RISC}\\ k_{ISC} & -k^T - \lambda\end{pmatrix}\right] = (k^S + \lambda)(k^T + \lambda) - k_{ISC}k_{RISC} = 0, \quad (16)$$

where E is the identity matrix. Eq. 16 can be rewritten as,

$$\lambda^2 + (k^S + k^T)\lambda + k^S k^T - k_{ISC}k_{RISC} = 0. \quad (17)$$

This quadratic equation provides λ as,

$$\lambda_{1,2} = -\frac{k^S + k^T}{2} \mp \sqrt{\frac{(k^S + k^T)^2}{4} - k^S k^T + k_{ISC}k_{RISC}}$$
$$= -\frac{1}{2}\left(k^S + k^T \pm \sqrt{(k^S - k^T)^2 + 4k_{ISC}k_{RISC}}\right). \quad (18)$$

Here, it is worth pointing out that $\lambda_1 < \lambda_2 < 0$ and, therefore, the exact prompt and delayed emission decays for the photoluminescence (k_p, k_d) are written as $k_p = -\lambda_1$ and $k_d = -\lambda_2$, respectively. Several rate equations introduced in the previous section have been derived from Eq. 18 but employ a number of different assumptions. Here, we note that Eq. 18 provides a relationship among k^S, k^T, k_p, and k_d as,

$$k^S + k^T = k_p + k_d. \quad (19)$$

Considering the clear relationships of $k^S > k_d$ and $k_p > k^T$, Eq. 16 implies the relationships of $k_p > k^S$ and $k^T > k_d$ (these provided relationships are explained again in later). If these relationships are not operative, then there should be no observed delayed emission. The corresponding eigenvectors are given by evaluating $\lambda_i\overrightarrow{v_i} = A\overrightarrow{v_i}$.

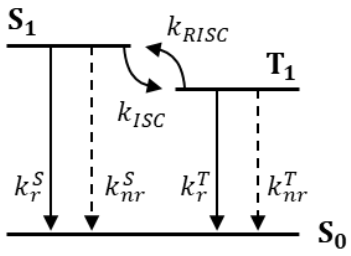

Figure 1. The scheme of photophysical process for three-state system.

$$\lambda_i \begin{pmatrix} x_1 \\ x_2 \end{pmatrix} = \begin{pmatrix} -k^S & k_{RISC} \\ k_{ISC} & -k^T \end{pmatrix} \begin{pmatrix} x_1 \\ x_2 \end{pmatrix}. \quad (20)$$

Eq. 20 leads to the relationship of Eq. 21.

$$\begin{cases} x_1 = \frac{k_{RISC}}{k^S + \lambda_i} x_2 \\ x_2 = \frac{k_{ISC}}{k^T + \lambda_i} x_1 \end{cases} \Leftrightarrow \begin{cases} x_1 = \frac{k_{RISC}}{k^S + \lambda_i} x_2 \\ x_2 = x_2, \quad x_2 \in \mathbb{R} \end{cases}$$
$$\Leftrightarrow \begin{cases} x_1 = x_1, \quad x_1 \in \mathbb{R} \\ x_2 = \frac{k_{ISC}}{k^T + \lambda_i} x_1 \end{cases}. \quad (21)$$

Using Eq 16, this set of equations can be easily reduced to a linear relationship between the dimensions of the eigenvector, allowing for the other dimension to be fixed to a freely chosen value. When $x_2 = 1$ is chosen, both eigenvectors, $\overrightarrow{v_1}$ and $\overrightarrow{v_2}$ are given by

$$\overrightarrow{v_1} = \begin{pmatrix} \frac{k_{RISC}}{k^S + \lambda_1} \\ 1 \end{pmatrix}, \qquad \overrightarrow{v_2} = \begin{pmatrix} \frac{k_{RISC}}{k^S + \lambda_2} \\ 1 \end{pmatrix}. \quad (22)$$

Inserting Eq. 22 in Eq. 15 yields the following equations for $[S_1]$ and $[T_1]$ as a function of time.

$$\begin{pmatrix} [S_1] \\ [T_1] \end{pmatrix} = c_1 \begin{pmatrix} \frac{k_{RISC}}{k^S + \lambda_1} \\ 1 \end{pmatrix} \exp(\lambda_1 t) + c_2 \begin{pmatrix} \frac{k_{RISC}}{k^S + \lambda_2} \\ 1 \end{pmatrix} \exp(\lambda_2 t), \quad (23)$$

$$\begin{cases} [S_1] = c_1 \frac{k_{RISC}}{k^S - k_p} \exp(-k_p t) + c_2 \frac{k_{RISC}}{k^S - k_d} \exp(-k_d t) \\ [T_1] = c_1 \exp(-k_p t) + c_2 \exp(-k_d t) \end{cases}. \quad (24)$$

The pre-exponential factors depend on the initial conditions. Using $[S_1] = [S_1]_{t=0}$ and $[T_1] = [T_1]_{t=0} = 0$ at $t = 0$, they are expressed as follows.

$$\begin{pmatrix} [S_1]_{t=0} \\ 0 \end{pmatrix} = c_1 \begin{pmatrix} \frac{k_{RISC}}{k^S - k_p} \\ 1 \end{pmatrix} + c_2 \begin{pmatrix} \frac{k_{RISC}}{k^S - k_d} \\ 1 \end{pmatrix}. \quad (25)$$

Eq. 25 expresses the relationship of Eq. 26.

$$\begin{cases} [S_1]_{t=0} = c_1 \frac{k_{RISC}}{k^S - k_p} + c_2 \frac{k_{RISC}}{k^S - k_d} \\ c_1 = -c_2 \end{cases}. \quad (26)$$

Here, $[S_1]_{t=0}$ and c_2 are given as Eqs. 27 and 28.

$$[S_1]_{t=0} = c_2 \frac{k_{RISC}(k_p - k_d)}{(k_p - k^S)(k^S - k_d)}, \quad (27)$$

$$c_2 = [S_1]_{t=0} \frac{k_{ISC}}{k_p - k_d}. \quad (28)$$

From Eqs. 24, 27, and 28, the exact $[S_1]$ and $[T_1]$ can be written as following equations.

$$[S_1] = \frac{[S_1]_{t=0}}{k_p - k_d}\left[(k^S - k_d)\exp(-k_p t) + (k_p - k^S)\exp(-k_d t)\right]. \quad (29)$$

$$[T_1] = \frac{[S_1]_{t=0} k_{ISC}}{k_p - k_d}\left[-\exp(-k_p t) + \exp(-k_d t)\right]. \quad (30)$$

Here, it is evident that Eq. 29 provides a bi-exponential decay of the S_1 population, and Eq. 30 provides a convex curve behavior of the evolution of the T_1 population. Hasse *et al.* reported that the emission decay of TADF materials corresponds to the S_1 population decay when assuming $k_r^T = k_{nr}^T = 0$.[12] They also verified that the depletion of the T_1 population was accurately determined by the TA decay. When now including the depletion from the T_1 state term described in Eq. 30, the total emission decay now includes the contributions from both S_1 and T_1 populations. Because the total emission from S_1 is the sum of the overall emission efficiencies from S_1 excitons, which are generated by direct photoexcitation and indirectly from the T_1 population, i.e., sum of prompt and delayed fluorescence ($\Phi_{PF} + \Phi_{DF}$), the contribution arising from generated triplet excitons must also be accounted for within the emission efficiency from T_1, phosphorescence (Φ_{Phos}). The S_1 and T_1 populations described by Eqs. 29 and 30 do not consider the luminescence. Therefore, the exact emission decay can be modelled as a bi-exponential decay as described in Eq. 31 using the radiative decay ratio for each exciton (Figure 2).

$$I(t) = \Phi_r^S[\mathrm{S_1}] + \Phi_r^T[\mathrm{T_1}] = \frac{[S_1]_{t=0}}{k_p - k_d}\begin{Bmatrix}\begin{bmatrix}(k^S - k_d)\Phi_r^S \\ -k_{ISC}\Phi_r^T\end{bmatrix}\exp(-k_p t) \\ +\begin{bmatrix}(k_p - k^S)\Phi_r^S \\ +k_{ISC}\Phi_r^T\end{bmatrix}\exp(-k_d t)\end{Bmatrix}. \quad (31)$$

where $I(t)$ is the time-dependent emission intensity, Φ_r^S and Φ_r^T are the quantum efficiencies of the radiative decay for S_1 and T_1 as written by and k_r^S/k^S and k_r^T/k^T, respectively. By using this equation that describes explicitly the emission decay, we can deeply understand the kinetics of TADF based on a three-state system.

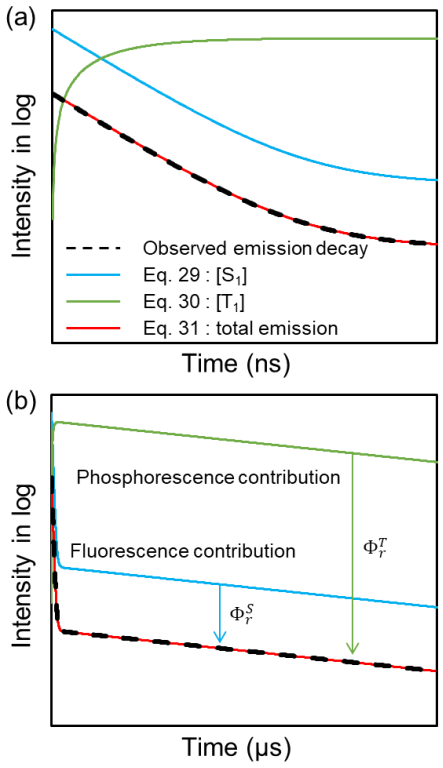

Figure 2. Emission decay curve and theoretical curves of Eqs. 29-31 within nanosecond time range (a) and microsecond time range (b). The difference of total emission and exciton population decays is related to the fluorescence and phosphorescence contributions depending on emitting ratio of each exciton.

Derivation of rate equations using steady-state approximation. In the previous section, we derived the rate equations for the emission decay of TADF materials based on a three-state system. In this section, we derive the rate equations by using the assumption of $k_r^S + k_{nr}^S + k_{ISC} \gg k_{RISC}$. This assumption implies that at least one of k_r^S, k_{nr}^S, or k_{ISC} is much larger than k_{RISC}. Since the T_1 level is lying below the S_1 level, $k_{ISC} \gg k_{RISC}$ should always be valid and no further assumptions are employed.

Before deriving the rate equations, we define Φ_{PF} and Φ_{DE} in terms of A_p, A_d, k_p and k_d which are parameters that describe a bi-exponential decay curve; these parameters are the pre-exponential factors (A) and decay rate constants (k) for the prompt (p) and delayed (d) components, respectively. There are several reported methods to obtain these values experimentally.[23] For instance, these values can be obtained from the integration of the emission decay corresponding to the prompt and delayed emission, respectively.[24] Also, there is the rough method of using the experimentally determined PLQY under aerated conditions as a surrogate for Φ_{PF}; however, the triplet state may not be completely quenched by O_2 under aerated conditions, and it is not the case that oxygen is benign to react with the S_1 state of TADF materials as its presence has been shown to increase the nonradiative decay path from the S_1 state.[25] The most commonly used approach to determine these values would be using Eqs. S3.1 and S3.2 where A_p, A_d, k_p and k_d can be obtained from bi-exponential curve fitting. However, the two exponential curves in Eq. 31 do not directly correspond to the exact "prompt emission" and "delayed emission", respectively. To estimate each efficiency, therefore, it is necessary to rewrite Eq. 31 as,

$$I(t) = (A_p + A_d)\exp(-k_p t) + A_d[-\exp(-k_p t) + \exp(-k_d t)]. \quad (32)$$

In this form, the first and second terms exactly correspond to the prompt and delayed emission, respectively (Figure 3). The quantum efficiency of the prompt (Φ_{PF}) and delayed emission (Φ_{DE}) are therefore given by,

$$\Phi_{PF} = \frac{\frac{A_p + A_d}{k_p}}{\frac{A_p + A_d}{k_p} + \frac{A_d}{k_d} - \frac{A_d}{k_p}}\Phi_{PLQY} = \frac{(A_p + A_d)k_d}{A_p k_d + A_d k_p}\Phi_{PLQY}, \quad (33)$$

$$\Phi_{DE} = \frac{\frac{A_d}{k_d} - \frac{A_d}{k_p}}{\frac{A_p + A_d}{k_p} + \frac{A_d}{k_d} - \frac{A_d}{k_p}}\Phi_{PLQY} = \frac{A_d(k_p - k_d)}{A_p k_d + A_d k_p}\Phi_{PLQY}, \quad (34)$$

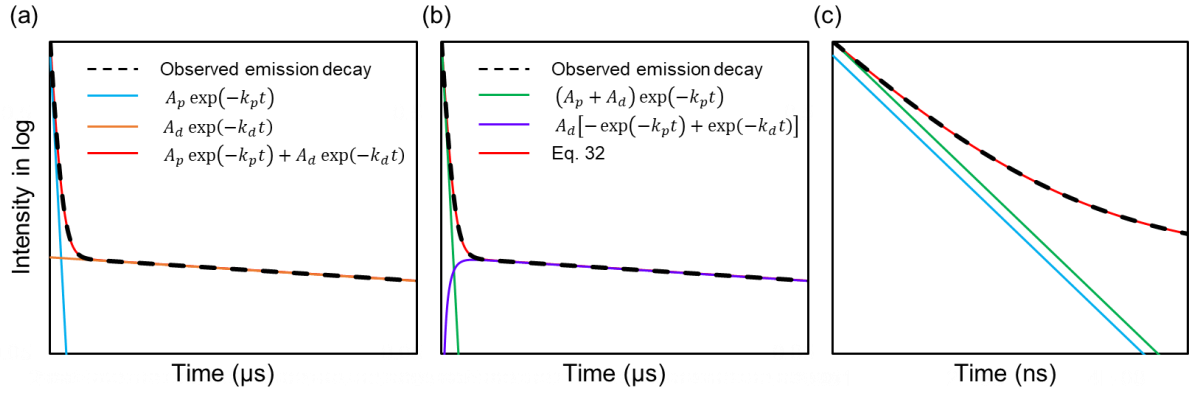

Figure 3. (a) Emission decay curve and biexponential fitting curves which are employed to estimate the prompt and delayed emission efficiency in general. (b) Corrected prompt and delayed component curves to provide exact emission efficiencies. (c) Closeup within nano second range to recognise difference of prompt components for general and corrected estimation method.

Under the assumption of $k_r^S + k_{nr}^S + k_{ISC} \gg k_{RISC}$ and with the restriction condition of $[S_1] \gg [T_1]$ ($t \ll 1/k_p$), the emission decay agrees with the prompt decay in this region and $[T_1]$ can be approximated to be 0 (Figure 2a). Eq. 12 can therefore be rewritten as Eq. 35. Hence, the singlet decay rate (k^S) can be approximated to the prompt decay rate (k_p), and the evolution of the S_1 population as a function of time at short time can be written as Eq. 36.

$$\frac{d[S_1]}{[S_1]} \approx -(k_r^S + k_{nr}^S + k_{ISC})dt. \tag{35}$$

$$\begin{aligned}[S_1] &\approx A_S \exp[-(k_r^S + k_{nr}^S + k_{ISC})t] \\ &= A_S \exp(-k^S t) \\ &\approx A_S \exp(-k_p t), \end{aligned} \tag{36}$$

where A_S is a pre-exponential factor.

Next, we focus on the exponential decay of $[T_1]$ to derive k_{ISC}. Eq. 13 can be rewritten as Eq. 37.

$$\frac{d[T_1]}{[T_1]} \approx -\left(k_r^T + k_{nr}^T + k_{RISC} - k_{ISC}\frac{[S_1]}{[T_1]}\right)dt. \tag{37}$$

Here, since $[S_1]$ and $[T_1]$ are time-dependent terms; this equation cannot be integrated. In the delayed decay region, however, we note that the decay rate is not exactly the same as the intrinsic triplet decay rate, as delayed emission decay also contains a term relating to the singlet population given that there is an $\exp(-k_d t)$ term found in the corresponding equations of Eqs. 29-31. Therefore, the ratio of singlet and triplet population, $[S_1]/[T_1]$, is not a time-dependent value but an exactly fixed value in the delayed decay region ($t \gg 1/k_p$). Further, the delayed component that originates from an S_1 population decay is extremely small compared with the T_1 population decay, $[T_1] \gg [S_1]$, because $k_{ISC} \gg k_{RISC}$ (Figure 2b). Therefore, the temporal differentiation of $[S_1]$ can be approximated to be 0, i.e., $d[S_1]/dt \approx 0$, in this time region. In other words, the population of the intermediate state S_1 resulting from upconversion of T_1 excitons, which then decay to S_0 can be considered using the steady-state approximation. We thus obtain the ratio of $[S_1]/[T_1]$ in Eq. 37 by using the steady-state approximation (SSA) in this time region. By the SSA, the ratio of $[S_1]/[T_1]$ can be provided as Eq. 38. Also, the SSA provides a description of the time dependence for $[T_1]$ as Eq. 39.

$$\frac{[S_1]}{[T_1]} \approx \frac{k_{RISC}}{k_r^S + k_{nr}^S + k_{ISC}} = \frac{k_{RISC}}{k^S}. \tag{38}$$

$$\begin{aligned}[T_1] &\approx A_T \exp\left\{-\left[k_r^T + k_{nr}^T + \left(1 - \frac{k_{ISC}}{k^S}\right)k_{RISC}\right]t\right\} \\ &= A_T \exp(-k_d t), \end{aligned} \tag{39}$$

where A_T is a pre-exponential factor for the delayed decay component of the triplet excitons. Now, k_d can be approximated as,

$$k_d \approx k_r^T + k_{nr}^T + \left(1 - \frac{k_{ISC}}{k^S}\right)k_{RISC}. \tag{40}$$

For this approximation, $k_r^S + k_{nr}^S + k_{ISC} \gg k_{RISC}$ remains a necessary assumption to achieve the restriction condition of $[T_1] \gg [S_1]$. However, this assumption is valid in general as we explained previously. Invoking the SSA leads to a reduction in the number of required assumptions for the analysis of the kinetics of organic TADF materials.

The total decay efficiency of singlet excitons generated by photoexcitation is the sum of Φ_r^S, Φ_{nr}^S, and Φ_{ISC} (for the distribution of singlet exciton, the ISC/RISC cycles are not considered because k^S was approximated as k_p in this section by Eq. 36, i.e., $\Phi_r^S \approx \Phi_{PF}$), and the decay efficiency of triplet excitons that results from an ISC process is the sum of Φ_r^T, Φ_{nr}^T, and Φ_{RISC}, which are given by

$$\Phi_r^S + \Phi_{nr}^S + \Phi_{ISC} = 1, \tag{41}$$

$$\Phi_r^T + \Phi_{nr}^T + \Phi_{RISC} = 1. \tag{42}$$

As a result of $k_r^S + k_{nr}^S + k_{ISC} \gg k_{RISC}$, the RISC process is rate determining for the decay of T_1 excitons via the S_1 state while the S_1 excitons generated by the RISC process rapidly decay to the S_0 state or return back to the T_1 state according to Eq. 31. In other words, the T_1 excitons return to T_1 state with a certain probability after ISC/RISC cycling. In this case, the efficiencies shown in Eq. 32 should be modified to take ISC/RISC cycling explicitly into account by using overall efficiencies (OEs), which correspond to the distributed exciton ratio between the S_1 and T_1 populations under the SSA via ISC/RISC cycles; these are $\Phi_r^{T\,OE} > \Phi_r^T$, $\Phi_{nr}^{T\,OE} > \Phi_{nr}^T$, and $\Phi_{RISC}{}^{OE} < \Phi_{RISC}$ (see section 4 in supporting information for the detailed relationship between efficiencies and OEs). From these, Φ_{ISC} can be divided into $\Phi_r^{T\,OE}$, $\Phi_{nr}^{T\,OE}$, and $\Phi_{RISC}{}^{OE}$, and the total efficiency is given by

$$\Phi_r^{T\,OE} + \Phi_{nr}^{T\,OE} + \Phi_{RISC}{}^{OE} = 1. \quad (43)$$

The fraction of T_1 exciton decays via S_1 ($\Phi_{ISC}\Phi_{RISC}{}^{OE}$) can be divided to occur either radiatively (Φ_r^S) or nonradiatively (Φ_{nr}^S), because $\Phi_{RISC}{}^{OE}$ encompasses the exciton ratio after considering ISC/RISC cycling. The delayed fluorescence (Φ_{DF}) can now be formulated as a function of the radiative fraction to the total efficiency, $\Phi_r^S + \Phi_{nr}^S$.

$$\begin{aligned}\Phi_{DF} = \Phi_{DE}R_{DE}^{DF} &= \Phi_{ISC}\Phi_{RISC}{}^{OE}\frac{\Phi_r^S}{\Phi_r^S + \Phi_{nr}^S} \\ &= \Phi_{ISC}\Phi_{RISC}{}^{OE}\frac{\Phi_r^S}{1-\Phi_{ISC}}. \end{aligned} \quad (44)$$

where Φ_{DE} are the quantum efficiency of phosphorescence and delayed emission, which is the sum of Φ_{DF} and phosphorescence (Φ_{Phos}), $\Phi_{DE} = \Phi_{DF} + \Phi_{phos}$. R_{DE}^{DF} is the ratio of the delayed fluorescence component of the delayed emission (Φ_{DF}/Φ_{DE}). On the other hand, the fraction of radiative decay from T_1 ($\Phi_{ISC}\Phi_r^{T\,OE}$) corresponds to Φ_{Phos}, as shown in Eq. 45.

$$\begin{aligned}\Phi_{ISC}\Phi_r^{T\,OE} &= \Phi_{Phos} \\ &= \Phi_{PLQY} - \Phi_{PF} - \Phi_{DF} \\ &= \Phi_{DE}(1 - R_{DE}^{DF}), \end{aligned} \quad (45)$$

In the three-state analysis, the lifetimes of TADF and phosphorescence are exactly the same since they occur from the same origin of the T_1 state (see Eq. 31). Therefore, both Φ_{DF} and Φ_{Phos} contribute to the delayed emission (Φ_{DE}). The total PL quantum yield (Φ_{PLQY}) is the sum of Φ_r^S and Φ_{DE}. Based on the above analysis, all of the efficiencies related to the TADF process are presented in Eqs. 46-51.

$$\Phi_r^S = \frac{k_r^S}{k_r^S + k_{nr}^S + k_{ISC}} = \frac{k_r^S}{k_p}. \quad (46)$$

$$\Phi_{nr}^S = 1 - \Phi_r^S - \Phi_{ISC} = \frac{k_{nr}^S}{k_r^S + k_{nr}^S + k_{ISC}} = \frac{k_{nr}^S}{k_p}. \quad (47)$$

$$\Phi_{ISC} = \frac{k_{ISC}}{k_r^S + k_{nr}^S + k_{ISC}} = \frac{k_{ISC}}{k_p}. \quad (48)$$

$$\Phi_r^{T\,OE} = \frac{\Phi_{Phos}}{\Phi_{ISC}} = \frac{k_r^T}{k_r^T + k_{nr}^T + (1-\Phi_{ISC})k_{RISC}} = \frac{k_r^T}{k_d}. \quad (49)$$

$$\Phi_{nr}^{T\,OE} = \frac{k_{nr}^T}{k_r^T + k_{nr}^T + (1-\Phi_{ISC})k_{RISC}} = \frac{k_{nr}^T}{k_d}. \quad (50)$$

$$\begin{aligned}\Phi_{RISC}{}^{OE} &= \frac{\Phi_{DF}(1-\Phi_{ISC})}{\Phi_r^S\Phi_{ISC}} \\ &= \frac{(1-\Phi_{ISC})k_{RISC}}{k_r^T + k_{nr}^T + (1-\Phi_{ISC})k_{RISC}} \\ &= \frac{(1-\Phi_{ISC})k_{RISC}}{k_d}. \end{aligned} \quad (51)$$

The corresponding rate constants are thus described by Eqs. 52-57.

$$k_r^S = k_p\Phi_{PF} = k_p\Phi_r^S. \quad (52)$$

$$k_{nr}^S = k_p\Phi_{nr}^S = k_p(1 - \Phi_r^S - \Phi_{ISC}). \quad (53)$$

$$k_{ISC} = k_p\Phi_{ISC}. \quad (54)$$

$$k_r^T = k_d\Phi_r^{T\,OE} = k_d\frac{\Phi_{Phos}}{\Phi_{ISC}} = k_d\frac{\Phi_{DE}(1-R_{DE}^{DF})}{\Phi_{ISC}}. \quad (55)$$

$$k_{nr}^T = k_d - (1-\Phi_{ISC})k_{RISC} - k_r^T. \quad (56)$$

$$k_{RISC} = k_d\frac{\Phi_{RISC}{}^{OE}}{1-\Phi_{ISC}} = \frac{k_pk_d}{k_{ISC}}\cdot\frac{\Phi_{DF}}{\Phi_r^S} = k_d\frac{\Phi_{DE}R_{DE}^{DF}}{\Phi_r^S\Phi_{ISC}}. \quad (57)$$

As explained above, we obtained these rate equations with essentially no assumptions; they are nearly identical to those described in Ref 7. The value of R_{DE}^{DF} can be obtained by fitting the delayed emission spectrum with the prompt fluorescence and phosphorescence spectra to provide the contribution of the phosphorescence to the delayed emission. However, we note that these equations still require Φ_{ISC} to be known. We can employ $\Phi_{nr}^S = 0$ or $\Phi_{nr}^T = 0$ as the limiting conditions to determine Φ_{ISC}. This method should be applicable for most TADF materials; however, it should be noted that the model employs the approximation of $k^S \approx k_p$ in this section, which introduces a degree of uncertainty to the estimated rate constants, thus reducing their accuracy.

Reevaluation of rate equation using assumption of $\Phi_{nr}^S = 0$ or $\Phi_{nr}^T = 0$. As it is difficult to measure directly k_{ISC}, in most of the literature the rate equations for TADF materials have been estimated using one of the assumptions of $\Phi_{nr}^S = 0$ or $\Phi_{nr}^T = 0$. The previously reported equations have been used indiscriminately to analyze not only highly emissive TADF materials but also poorly emissive materials, despite the inappropriateness of these models to handle the latter given their implicit assumptions. The derived rate constants must therefore be evaluated skeptically. The equations provided in the previous section using the SSA have upward compatibility with previously reported models, especially those of Goushi-Masui and Dias, which have been often employed in the literature.[8,10] When we employ $\Phi_{nr}^S = 0$ or $\Phi_{nr}^T = 0$ as a limiting condition to obtain Φ_{ISC}, our equation using SSA leads to the same rate equations as those discussed in Refs 8 and 10 ($\Phi_{Phos} \approx 0$), respectively, shown here as Eqs. 58 and 59.

$$\Phi_{ISC}^{nrS=0} = 1 - \Phi_{PF}. \quad (58)$$

$$\Phi_{ISC}^{nrT=0} = \frac{\Phi_{DE} - \Phi_{Phos}(1-\Phi_{PF})}{\Phi_{PF} + \Phi_{DE} - \Phi_{Phos}}. \quad (59)$$

Where $\Phi_{ISC}^{nrS=0}$ and $\Phi_{ISC}^{nrT=0}$ correspond to the maximum and minimum values of Φ_{ISC}, respectively. When $\Phi_r^T \approx 0$ (this approximation holds for organic TADF emitter behavior at around room temperature), the average k_{ISC} and k_{RISC} values within the range between these limiting conditions ($k_{ISC}^{Avg.}$ and $k_{RISC}^{Avg.}$, respectively) are provided as follows.

$$k_{ISC}^{Avg.} = \frac{k_p}{2}\cdot\frac{\left[\Phi_{PLQY}(1-\Phi_{PF}) + \Phi_{DF}\right] \pm \left[\Phi_{PF}\left(1-\Phi_{PLQY}\right)\right]}{\Phi_{PLQY}}. \quad (60)$$

$$k_{RISC}^{Avg.} = \frac{k_d}{2}\cdot\frac{\left[\Phi_{PLQY}(1-\Phi_{PF}) + \Phi_{DF}\right] \pm \left[\Phi_{PF}\left(1-\Phi_{PLQY}\right)\right]}{\Phi_{PF}(1-\Phi_{PF})}. \quad (61)$$

The maximum and minimum values of $k_{ISC}^{Avg.}$ are the values for the limiting conditions of $\Phi_{nr}^S = 0$ and $\Phi_{nr}^T = 0$, respectively, while the maximum and minimum values of $k_{RISC}^{Avg.}$ are the values for the limiting conditions of $\Phi_{nr}^T = 0$ and $\Phi_{nr}^S = 0$, respectively.

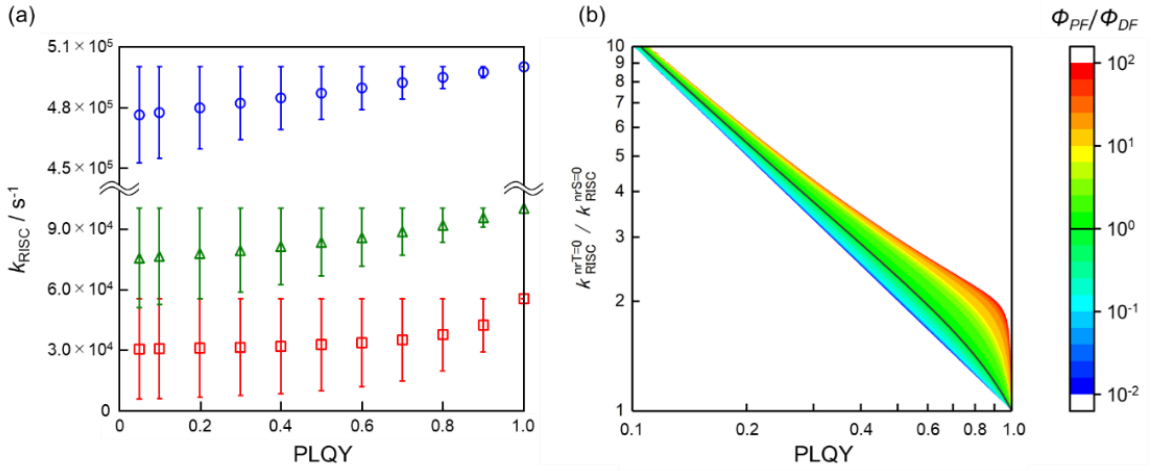

Figure 4. (a) Plot of $k_{RISC}^{Avg.}$ for the delayed emission ratio to PLQY; blue circle, $\Phi_{PF}:\Phi_{DF} = 0.1:0.9$; green triangle, $\Phi_{PF}:\Phi_{DF} = 0.5:0.5$; red square, $\Phi_{PF}:\Phi_{DF} = 0.9:0.1$; $1/k_p$, 20 ns; $1/k_d$, 20 μs; plot was generated using Eq. 61. (b) Ratio of RISC rate constant between assuming $k_{nr}^S = 0$ and $k_{nr}^T = 0$ for each PLQY with color properties indicating the ratio of Φ_{PF} and Φ_{DF}; solid black line, $\Phi_{PF}:\Phi_{DF} = 1$; plot was generated by using Eq. 61.

We analysed the range of k_{RISC} values of the three-state system by using Eq. 61. Figure 4a shows the plot of $k_{RISC}^{Avg.}$ for the delayed emission ratio as a function of PLQY. The maximum and minimum values of the ranges are the values for the limiting conditions of $\Phi_{nr}^T = 0$ and $\Phi_{nr}^S = 0$, respectively. The plots of blue circles, green triangles, and red squares correspond to the respective values of 0.9, 0.5, and 0.1 for Φ_{DF}. The prompt and delayed emission lifetimes (τ_p and τ_d) were fixed at 20 ns and 20 μs, which are representative values observed for organic TADF emitters. This plot reveals several important points: (1) the ratio of the delayed emission component significantly affects the magnitude of k_{RISC}. When the emission decay has only a small contribution from the delayed component, k_{RISC} is not only slow but remains slow even if the material shows a high PLQY; (2) When the PLQY of TADF materials is not very high, i.e., less than 0.8, there is a larger range of accessible k_{RISC} values within the limiting conditions, regardless of the magnitude of Φ_{DE}. Similar relationships also exist with respect to k_{ISC}. It is important to note that the assumption of $\Phi_{nr}^S = 0$ results in both an underestimation of k_{RISC} and an overestimation of k_{ISC} while the assumption of $\Phi_{nr}^T = 0$ results in both an overestimation of k_{RISC} and an underestimation of k_{ISC}. The estimated k_{RISC} values do not change as a result of changes to the PLQY when the assumption of $\Phi_{nr}^T = 0$ is employed. This in turn creates problems when this assumption is applied to the poorly emissive TADF materials. Especially for inefficient emitters ($\Phi_{PLQY} < 0.1$), the values of k_{RISC} under the assumption of $\Phi_{nr}^S = 0$ or $\Phi_{nr}^T = 0$ have been estimated with one order magnitude higher error depending on the ratio of Φ_{PF} and Φ_{DF} (Figure 4b). Further, despite when materials have high PLQY ($\Phi_{PLQY} > 0.9$), the difference between $k_{RISC}^{nrS=0}$ and $k_{RISC}^{nrT=0}$ can be more than double than the Φ_{PF}/Φ_{DF} ratio. In the supporting information, several equations are provided to convert k_{ISC} and k_{RISC} using a limiting condition to another condition or average rate constants, e.g. these equation make possible to interconvert the rate constants defined with the models of either Goushi-Masui or Dias and our models. When the k_p and k_d are each provided in the literature along with Φ_{PLQY}, Φ_{PF}, and Φ_{DF}, Eqs. 59 and 60 allow direct extrapolation of the range of accessible values of k_{ISC} and k_{RISC}, and make possible the comparison between the value estimated using the different models and thus assess the possible range of values these rate constants can attain.

Recently, the importance of the role of intermediate triplet excited states in facilitating RISC processes, aided by spin-vibronic coupling has been elucidated.[26-29] Thus, we often find the delayed component of TADF shows biexponential decay. Naito *et al.* demonstrated the direct fitting of the TR PL decay by using the rate constants as a fitting parameter within a four-state model.[27] Very recently, we also reported a rate analysis based on a four-state system consisting of S_1, T_1, T_n, and S_0, where T_n is a triplet state of intermediate energy between S_1 and T_1.[30] The rate equations for the four-state system implicate that RISC proceeds via transient population of the intermediate T_n state. However, it is difficult to derive the exact rate equations for the four-state analysis without invoking several *a priori* assumptions. Such a four-state system can also be modeled by using the SSA in a similar manner as we have described for the three-state system (see section 15 in supporting information). There are two required assumptions: the direct ISC/RISC process between the S_1 and T_1 states and the direct radiative/nonradiative processes from T_n to S_0 be both forbidden, which are related to El-Sayed's and Kasha's rules, respectively.[31,32] This situation occurs when S_1 and T_1 involve orbitals of the same orbital type and thus the corresponding ISC/RISC rate constants are negligibly small. Using a similar approach to that employed for the three-state system, we can obtain the rate equations that describe all of the rate constants, k_r^S, k_{nr}^S, k_{ISC}, k_{RISC}, k_{IC}^T, k_{RIC}^T, and k_{nr}^T. Here, k_{IC}^T and k_{RIC}^T are the forward (IC) and reverse internal conversion (RIC) rate constants between T_n and T_1. We again confront the problem of determining Φ_{ISC}. As explained in the previous section, we wish to avoid invoking the assumption that $\Phi_{nr}^S = 0$ or $\Phi_{nr}^T = 0$ in order to estimate Φ_{ISC}. Therefore, we propose to determine Φ_{ISC} using, again, the average rate constants for the ISC, RISC, IC and RIC processes within a range of accessible

values as an alternative, assuming $\Phi_{nr}^{S} = 0$ or $\Phi_{nr}^{T} = 0$. When $\Phi_{r}^{T} \approx 0$ is employed as a likely limiting condition, in an analogous manner to our previous analysis, k_{ISC}, k_{RISC}, k_{IC} and k_{RIC} values within these conditions are given by Eqs. 62-65.

$$k_{ISC}^{Avg.} = \frac{k_p \begin{bmatrix} 2\Phi_{PLQY} - \Phi_{PF}(1+\Phi_{PLQY}) \\ \pm\Phi_{PF}(1-\Phi_{PLQY}) \end{bmatrix}}{2\Phi_{PLQY}}. \quad (62)$$

$$k_{RISC}^{Avg.} = \frac{k_{d1}\Phi_{DF1} \begin{bmatrix} 2\Phi_{PLQY} - \Phi_{PF}(1+\Phi_{PLQY}) \\ \pm\Phi_{PF}(1-\Phi_{PLQY}) \end{bmatrix}}{2\Phi_{PF}(1-\Phi_{PF})(\Phi_{PLQY}-\Phi_{PF})}. \quad (63)$$

$$k_{IC}^{Avg.} = k_{d1} - \frac{k_{d1}\Phi_{DF1} \begin{bmatrix} 1+\Phi_{PLQY} - 2\Phi_{PF} \\ \pm(1-\Phi_{PLQY}) \end{bmatrix}}{2(1-\Phi_{PF})(\Phi_{PLQY}-\Phi_{PF})}. \quad (64)$$

$$k_{RIC}^{Avg.} = \frac{k_{d2} \begin{bmatrix} 2\Phi_{DF2}(1-\Phi_{PF}) + \Phi_{DF1}(1-\Phi_{PLQY}) \\ \pm\Phi_{DF1}(1-\Phi_{PLQY}) \end{bmatrix}}{2\Phi_{DF1}(1-\Phi_{PF}-\Phi_{DF1})}. \quad (65)$$

Derivation of exact rate equations for three-state system containing k_{ISC}. In first section, we derived the exact equation to model the experimental bi-exponential emission decay of TADF materials. In second section, we also provided a solution to determine the rate equations while minimizing the assumptions made. Though these rate equations provide several important insights, they are still based on the approximation of $k^S \approx k_p$. Here, we show that this approximation need not be invoked and derive the exact rate equations. In so doing, we aim to eliminate the confusion caused by implicating this approximation.

Here, we focus on the exponential decay of $[T_1]$ to derive k_{ISC}. In second section, we obtained the ratio of $[S_1]/[T_1]$ by applying the SSA to Eq. 12, but the exact value of $[S_1]/[T_1]$ within the delayed emission regime can be provided from the exact population decay equations of Eqs. 29 and 30.

$$\frac{[S_1]}{[T_1]} = \frac{k_p - k^S}{k_{ISC}} = \frac{k_{RISC}}{k^S - k_d}. \quad (66)$$

Therefore, Eq. 37 can be integrated and the evolution of $[T_1]$ as a function of time becomes,

$$[T_1] = A_d^T \exp\left\{-\left[k_r^T + k_{nr}^T + \left(1 - \frac{k_{ISC}}{k^S - k_d}\right)k_{RISC}\right]t\right\} = \frac{[S_1]_{t=0}k_{ISC}}{k_p - k_d}\exp(-k_d t), \quad (67)$$

where A_d^T is a preexponential factor of the delayed decay of triplet excitons. Therefore, k_d can be written by,

$$k_d = k_r^T + k_{nr}^T + \left(1 - \frac{k_{ISC}}{k^S - k_d}\right)k_{RISC}. \quad (68)$$

From the relationship of Eqs. 19 and 68, k_p can be written by

$$k_p = k_r^S + k_{nr}^S + \left(1 + \frac{k_{RISC}}{k^S - k_d}\right)k_{ISC}. \quad (69)$$

Surprisingly, Eq. 69 implies that k_{ISC} is slightly accelerated by the presence of multiple ISC/RISC cycles, and the resulting relationship of the observed decay rate of S_1 (k_p) is larger than the pure decay rate of S_1 (k^S), in spite of increasing the singlet exciton population due to the upconversion from a T_1 state. The relationship $k_p > k^S$ was mentioned also in first section. This phenomenon would be the result of the inflow from T_1. From the relationship of Eqs. 16, 68 and 69, the overall efficiency of ISC and RISC ($\Phi_{ISC}{}^{OE}$, $\Phi_{RISC}{}^{OE}$) can be written as,

$$\Phi_{ISC}{}^{OE} = \frac{\left(1 + \frac{k_{RISC}}{k^S - k_d}\right)k_{ISC}}{k_p} = \frac{k_{ISC} + k_p - k^S}{k_p}, \quad (70)$$

$$\Phi_{RISC}{}^{OE} = \frac{\left(1 - \frac{k_{ISC}}{k^S - k_d}\right)k_{RISC}}{k_d} = \frac{k_{RISC} - k_p + k^S}{k_d}. \quad (71)$$

Because Φ_{DF} can be explained as the overall emission efficiency from S_1 via T_1, it can be defined as,

$$\Phi_{DF} = \Phi_{DE}R_{DE}^{DF} = \Phi_{ISC}{}^{OE}\Phi_{RISC}{}^{OE}\frac{\Phi_{PF}}{1 - \Phi_{ISC}{}^{OE}} = \frac{k_r^S}{k^S - k_{ISC}}\Phi_{ISC}{}^{OE}\Phi_{RISC}{}^{OE}, \quad (72)$$

where Φ_{PF} corresponds to the overall quantum efficiency of the radiative decay from excitons populated directly at S_1. Note that the generated S_1 excitons via T_1 described as $\Phi_{ISC}{}^{OE}\Phi_{RISC}{}^{OE}$ decay to S_0 both radiatively or nonradiatively because $\Phi_{ISC}{}^{OE}\Phi_{RISC}{}^{OE}$ is the final distributed exciton ratio of S_1 via T_1, considering the ISC/RISC cycles. They should not distribute to T_1 anymore. From Eq. 72, the quadratic equation for k_{ISC} can be obtained as

$$k_{ISC} = \frac{-b - \sqrt{b^2 - 4ac}}{2a}, \quad (73)$$

$$a = k_d\frac{\Phi_{DE}}{\Phi_{PF}}R_{DE}^{DF} - k_p + k^S, \quad (74)$$

$$b = (k_p - k^S)(k^S - k_p - k_d) - ak^S, \quad (75)$$

$$c = (k_p - k^S)^2(k^S - k_d). \quad (76)$$

As k_{ISC} should be smaller than k^S, the value is uniquely determined as described in Eq. 73. When we can approximate that the delayed emission does not contain phosphorescence ($R_{DE}^{DF} \approx 1$), the value of a becomes 0 and the equation for k_{ISC} can be rewritten more simply as,

$$k_{ISC} = \frac{(k_p - k^S)(k^S - k_d)}{k_d + k_p - k^S}. \quad (77)$$

k_{RISC} can be obtained from the relationship shown in Eq. 78, which is also found in Eq. 16. The equation for k_{RISC} is provided as Eq. 79 with the approximation of $R_{DE}^{DF} \approx 1$.

$$k_{RISC} = \frac{(k_p - k^S)(k^S - k_d)}{k_{ISC}}. \quad (78)$$

$$k_{RISC} = k_d + k_p - k^S. \quad (79)$$

From Eq. 31, Eq. 33 can be rewritten by,

$$\frac{\Phi_{PF}}{\Phi_{PLQY}} = \frac{(A_p + A_d)k_d}{A_p k_d + A_d k_p} = \frac{\Phi_r^S(k_p - k_d)k_d}{[\Phi_r^S(k^S - k_d) - \Phi_r^T k_{ISC}]k_d + [\Phi_r^S(k_p - k^S) + \Phi_r^T k_{ISC}]k_p}. \quad (80)$$

Eq. 80 provides an exact solution for the singlet decay rate (k^S) as,

$$k^S = k_p - k_d\frac{\Phi_{DE}}{\Phi_{PF}} + k_{ISC}\frac{\Phi_r^T}{\Phi_r^S}. \quad (81)$$

This equation also can be derived from Eqs. 31 and 34 with the similar derivation, and also the ratio of preexponential factor (A_d/A_p) of Eq. 31. When $R_{DE}^{DF} \approx 1$ can be approximated meaning no phosphorescence in emission, k^S is simplified as the phosphorescence related term vanishes as Eq. 82.

$$k^S = k_p - k_d\frac{\Phi_{DF}}{\Phi_{PF}}. \quad (82)$$

The rate constants for non-radiative decay from S_1 and T_1 can be extracted from Eq. 19 without invoking the simplification of $R_{DE}^{DF} \approx 1$ as,

$$k_{nr}^S = k^S - k_r^S - k_{ISC}, \quad (83)$$

$$k_{nr}^T = k^T - k_{RISC} - k_r^T = k_d + k_p - k^S - k_{RISC} - k_r^T. \quad (84)$$

When data is collected at 300 K or in solution state, it is not unusual to assume the observed emission does not contain phosphorescence ($\Phi_{Phos} \approx 0$), i.e., $R_{DE}^{DF} \approx 1$. However, k_{nr}^T is always 0 when approximated as $R_{DE}^{DF} \approx 1$ because of Eqs. 79 and 84. As a result, the rate constants for k_{nr}^S, k_{ISC}, and k_{RISC} under the approximation of $R_{DE}^{DF} \approx 1$ can be written in terms of decay rates and efficiencies for prompt and delayed components as shown in Eqs. 85-87. In this case, it should be noted that k_{RISC} is obtained as a maximum for these possible values.

$$k_{nr}^S = k_p\frac{\Phi_{PF}}{\Phi_{PLQY}}(1 - \Phi_{PLQY}), \quad (85)$$

$$k_{ISC} = k_p\frac{\Phi_{DF}}{\Phi_{PLQY}} - k_d\frac{\Phi_{DF}}{\Phi_{PF}}. \quad (86)$$

$$k_{RISC} = k_d\frac{\Phi_{PLQY}}{\Phi_{PF}}. \quad (87)$$

Interestingly, the rate equation for k_{RISC} is exactly same with the model of Dias. The radiative decay rate k_r^S is independently obtained by,

$$k_r^S = k_p\Phi_{PF}. \quad (88)$$

Next, we provide the exact solution of the kinetics analysis for TADF of a three-state system without any assumptions and approximations. The relationship related to the phosphorescence is provided as,

$${\Phi_{ISC}}^{OE}{\Phi_r^T}^{OE} = \Phi_{Phos} = \Phi_{PLQY} - \Phi_{PF} - \Phi_{DF} = \Phi_{DE}(1 - R_{DE}^{DF}), \quad (89)$$

From Eq. 89 the rate equation and radiative decay quantum efficiency for T_1 excitons (k_r^T and Φ_r^T) can be described as Eqs. 90 and 91.

$$k_r^T = \frac{k_d\Phi_{DE}(1 - R_{DE}^{DF})}{{\Phi_{ISC}}^{OE}} = \frac{k_p k_d\Phi_{DE}(1 - R_{DE}^{DF})}{k_{ISC} + k_p - k^S}. \quad (90)$$

$$\Phi_r^T = \frac{k_d{\Phi_r^T}^{OE}}{k^T{\Phi_{ISC}}^{OE}} = \frac{k_p k_d\Phi_{DE}(1 - R_{DE}^{DF})}{(k_p + k_d - k^S)(k_{ISC} + k_p - k^S)}. \quad (91)$$

From the Eqs. 81, 88, 89, and 89 the exact k^S can be obtained as a solution of the following cubic equation,

$${k^S}^3 + d{k^S}^2 + ek^S + f = 0. \quad (92)$$

$$d = -\left[k_{ISC} + 3k_p + k_d\left(1 - \frac{\Phi_{DE}}{\Phi_{PF}}\right)\right]. \quad (93)$$

$$e = k_{ISC}k_d\left[1 - \frac{\Phi_{DE}}{\Phi_{PF}}(2 - R_{DE}^{DF})\right] - k_p(3k_p + 2d) - {k_d}^2\frac{\Phi_{DE}}{\Phi_{PF}}. \quad (94)$$

$$f = -(k_{ISC} + k_p)(k_p + k_d)\left(k_p - k_d\frac{\Phi_{DE}}{\Phi_{PF}}\right). \quad (95)$$

Because k^S should be smaller than k_p and larger than k_{ISC} ($k_{ISC} < k^S < k_p$), the solution to the cubic equation is uniquely determined using the Cardano–Tartaglia formula as,

$$k^S = \frac{-1 + i\sqrt{3}}{2} \times \sqrt[3]{-g + \sqrt{g^2 + h^3}} + \frac{-1 - i\sqrt{3}}{2} \times \sqrt[3]{-g - \sqrt{g^2 + h^3}} - \frac{1}{3}d. \quad (96)$$

$$g = \frac{27f + 2d^3 - 9de}{54}. \quad (97)$$

$$h = \frac{3e - d^2}{9}. \quad (98)$$

Because the exact equations for k_{ISC} and k^S contain the terms of k^S and k_{ISC}, respectively, a numerical analysis is required to obtain the exact rate. For example, k_{ISC} at $R_{DE}^{DF} \approx 1$ can be provided to obtain k^S and then estimated k_{ISC} were evaluated to avoid the circular reference; a new k_{ISC} value can be provided to minimize the difference between the given and estimated values. The R_{DE}^{DF} is given as all rate constants are provided as ≥ 0.

Here, we derived the exact rate equations for organic TADF materials based on the three-state model. It is noteworthy that the equations in this section considerably reduce the errors in the estimation of the rate constants compared with the previous methods without the requirement of additional experiments except the transient PL decay and PLQY measurements to obtain k_{ISC}. The equation for k_{ISC} cannot be applied to the previously reported rate equations that use the approximation of $k^S \approx k_p$. We note here again, the emission lifetimes of TADF and phosphorescence are exactly the same as in the three-state system because both decays are related to the T_1 decay; the ISC/RISC cycles behave as an exciton pool for both decays. Therefore, the delayed emission should always include both contributions from delayed fluorescence and phosphorescence at the fixed ratio (R_{DE}^{DF} and $1 - R_{DE}^{DF}$) in the three-state model. In other words, when data contain three or more decays, the "exact" rate equation derived in this section should not be applied. For example, phosphorescence often can be found as an additional radiative decay distinct from TADF. In this case, the material should be analyzed by other models, e.g., four-state model explained in *SI* of this paper. Because the rate equations describing the three-state system were derived considering the phosphorescence is intrinsic to the delayed

emission, it is favorable to collect the emission decay data in the full-range of fluorescence and phosphorescence spectra, i.e., the decay data collected not only by a single wavelength measurement but also with multiple wavelength measurements. When the single wavelength measurement is employed, the measurement wavelength should be a wavelength around the intersection between the normalized fluorescence and phosphorescence spectra.

Finally, we re-estimated the rate constants for several TADF materials in the literature: 4CzIPN;[28] 5CzBN;[28,33] 3Cz2DPhCzBN;[33] 5Cz-TRZ;[34] TQ;[35] ν-DABNA;[36] TMCz-BO;[37] TPAt-tFFO;[12] Br-3PXZ-XO;[38] DiKTa;[39] and MCz-TXT.[40] We undertook this analysis with the approximation of $R_{DE}^{DF} \approx 1$. The rate constant values listed in Table 1 contain the originally reported values from the literature, the values using the equations where the SSA is invoked with the general estimation method of Φ_{PF} and Φ_{DE} (SSA-1), the values using equations where the SSA is invoked with the corrected estimation method of Φ_{PF} and Φ_{DE} (SSA-2), and using the "exact" equations for the three-state model. For SSA-1 and SSA-2, the k_{ISC} and k_{RISC} values are provided with the limiting conditions of $k_{nr}^{S} = 0$ and $k_{nr}^{T} = 0$.

An evaluation of the results using these different models reveals that the literature reported k_{RISC} values and those using SSA-1 are similar. Most of the literature reported k_{RISC} values using the assumption of $k_{nr}^{S} = 0$ and those using the exact value ($k_{nr}^{T} = 0$) show no difference; however, this is the result of a fortuitous cancellation of errors with the assumption of $k_{nr}^{S} = 0$, the approximation of $k^{S} \approx k_p$, and the estimation method of Φ_{PF} and Φ_{DE}. The k_{RISC} values of TPAt-tFFO, which is estimated with the assumption of $k_{nr}^{T} = 0$, show relatively large differences depending on the model used. This is related to the estimation method of Φ_{PF} and Φ_{DE} and the use of the approximation via a Maclaurin expansion. For the k_{RISC} estimation, the SSA-2 with the condition of $k_{nr}^{T} = 0$ showed good agreement with those using the exact equation. This is because both rate equations to determine k_{RISC} are exactly the same (see Eqs. 87 and S7.5) when approximating $R_{DE}^{DF} \approx 1$ and when using SSA with the limiting condition of $k_{nr}^{T} = 0$. When TADF materials show very fast T_1-S_1 upconversion, i.e. $k_p \approx k_d$, will become available, the equations using the SSA cannot be applied, but there remains no restriction to the use of the exact equations. In addition, when using the wrong estimation of Φ_{PF} and Φ_{DE} by Eqs. S3.1 and S3.2 employed in many literature reports, k_{ISC} tended to be overestimated; this can be found by comparing the k_{ISC} between SSA-1 and SSA-2. To reduce the estimation error of the rate constants, it is important to use the corrected estimation method for Φ_{PF} and Φ_{DE}. Further, Eqs. 86 and S6.4 provide the correction coefficient, $-k_d\,\Phi_{DF}/\Phi_{PF}$ for k_{ISC} to exclude the affection of $k^{S} \approx k_p$. Thus, all derived equations help understand the spin-flip processes with the exact rate constants for reported TADF materials; the equations in the model with practically no assumptions allow the conversion of the rate constants obtained using the model of Goushi-Masui's to those using the model of Dias, and the correction coefficient between the model of Dias and exact model provides the exact rate constants.

As an additional finding, the estimated rate constants numerical analysis showed no change with the case of $R_{DE}^{DF} \approx 1$ for most of the materials explained above. Both k_r^T and k_{nr}^T are estimated as $\ll 1$. Therefore, the approximation of $R_{DE}^{DF} \approx 1$ should be reasonable. This finding is highly suggestive in the photophysics in three-state system. When there is the decay channel of T_1 via S_1, then direct decay from T_1 to S_0 is not available. To explain the direct decay of T_1, a new model would be necessary to explain the materials that show the dual emission of TADF and room temperature phosphorescence. The four-state kinetics analysis explained in the *SI* would help to understand the advanced function of emissive materials.

Summary

In this paper, we provided the exact decay curve equation for the TADF materials on the three-state system. The equation was derived from exact S_1 and T_1 population decays considering all exciton decay processes. The exact equations of exciton population decays help advance our understanding of the photophysics of not only TADF materials but also materials related to the three-state system of S_1, T_1, and S_0, because these equations were derived without employing any approximations and assume not particular preferential decay pathway. In addition, the equations to estimate the efficiencies for the prompt and delayed emission components (Φ_{PF} and Φ_{DE}) were corrected. The estimation method of efficiencies strongly influenced the estimated value of rate constants. Further, we demonstrated that it is possible to derive the rate equations with "practically" and "perfectly" no-assumptions. The rate equations are summarized in Table 2 (Entry 1-4).

For the first method, we employed two approximations. One is $k^{S} \approx k_p$, which is commonly used, to analyse the prompt emission under the condition of $[S_1] \gg [T_1]$ ($t \ll 1/k_p$). This approximation requires the assumption of $k_r^S + k_{nr}^S + k_{ISC} \gg k_{RISC}$; however, this is satisfied because of the relationship of exo- and endothermic processes of k_{ISC} and k_{RISC}. The other one is the steady-state approximation of the S_1 population to obtain the $[S_1]/[T_1]$ ratio at the delayed emission region of $[S_1] \ll [T_1]$ ($t \gg 1/k_p$). This approximation also requires the assumption of $k_r^S + k_{nr}^S + k_{ISC} \gg k_{RISC}$. To analyse the experimental data, this method requires that the Φ_{ISC} must be provided by additional measurement; however, it is possible to employ $\Phi_{nr}^{S} = 0$ or $\Phi_{nr}^{T} = 0$ as not assumptions but as limiting conditions. This practically no-assumption method makes exchange these two assumptions used in the most of literatures being able to compare the reported values. This method has some margin of error; however, it should be noted that there are some inapplicable cases because of the approximations employed. When Φ_{ISC} is not provided, the rate constants should be reported as average values between both sets of limiting conditions. In addition, the rate equations for the TADF materials using a four-state system of S_0, S_1, T_n and T_1 are derived in the supporting information.

Table 1. Rate constants of interest TADF materials in this paper for three-state TADF system (assuming $R_{DE}^{DF} \approx 1$).

		Φ_{PF}	Φ_{DF}	k_p (10^7 s^{-1})	k_d (10^5 s^{-1})	k_r^S (10^7 s^{-1})	k_{nr}^S (10^6 s^{-1})	k_{ISC} (10^7 s^{-1})	k_{nr}^T (10^4 s^{-1})	k_{RISC} (10^5 s^{-1})
4CzIPN in toluene	original	0.21[a]	0.65	8.850	2.174	1.8	-	7.0	-	8.8
	SSA-1	0.21[a]	0.65			1.858	0	6.991	3.853	8.517
						1.858	3.025	6.689	0	8.903
	exact	0.21[a]	0.65			1.858	3.190	6.61	0	8.836
5CzBN in toluene	original	0.07[a]	0.68	26.32	0.214	1.9	-	25	-	2.2
	SSA-1	0.07[a]	0.68			1.842	0	24.47	0.574	2.232
						1.842	6.140	23.86	0	2.289
	exact	0.07[a]	0.68			1.842	6.160	23.84	0	2.288
5CzBN 20 wt% in mCBP	original	0.16	0.65	31.25	0.980	5.0	-	26	4.1	3.6
	SSA-1	0.16	0.65			5.000	0	26.24	2.218	4.730
						5.000	11.73	25.07	0	4.952
	SSA-2	0.160	0.650			5.006	0	26.24	2.218	4.735
						5.006	11.74	25.07	0	4.957
	exact	0.160	0.650			5.006	11.74	25.03	0	4.957
3Cz2DPhCzBN 20 wt% in mCBP	original	0.14	0.80	22.22	1.770	3.0	-	19	4.1	9.9
	SSA-1	0.14	0.80			1.552	0	19.11	1.235	11.76
						1.552	19.86	18.91	0	11.88
	SSA-2	0.141	0.799			3.125	0	19.10	1.236	11.717
						3.125	19.95	18.90	0	11.83
	exact	0.141	0.799			3.125	19.95	18.80	0	11.83
5Cz-TRZ in toluene	original	0.031	0.889	24.39	2.439	0.544	-	17	-	150
	SSA-1	0.031	0.889			0.544	0	17.00	4.345	155.8
						0.544	0.473	16.95	0	156.2
	SSA-2	0.034	0.886			0.591	0	16.95	4.357	143.4
						0.591	0.514	16.90	0	143.8
	exact	0.034	0.886			0.591	0.514	15.52	0	143.8
TQ 10 wt% in DPEPO	original	0.459	0.095	8.8	111	-	-	-	-	0.035
	SSA-1	0.459	0.095			5.216	0	6.148	0.743	0.034
						5.216	41.99	1.949	0	0.109
	SSA-2	0.459	0.095			5.216	0	6.148	0.743	0.034
						5.216	41.99	1.948	0	0.109
	exact	0.459	0.095			5.216	41.99	1.948	0	0.109

		Φ_{PF}	Φ_{DF}	k_p (10^7 s^{-1})	k_d (10^5 s^{-1})	k_r^S (10^7 s^{-1})	k_{nr}^S (10^6 s^{-1})	k_{ISC} (10^7 s^{-1})	k_{nr}^T (10^4 s^{-1})	k_{RISC} (10^5 s^{-1})
ν-DABNA in toluene	original	0.82	0.08	24.39	2.439	20	22	2.3	0	2.0
	SSA-1	0.82	0.08			20.00	0	4.390	13.55	1.322
						20.00	22.22	2.168	0	2.677
	SSA-2	0.820	0.080			20.00	0	4.388	13.56	1.321
						20.00	22.22	2.166	0	2.677
	exact	0.820	0.080			20.00	22.22	2.163	0	2.677
TMCz-BO 30 wt% in PPF	original	0.66	0.32	2.632	13.33	1.7	-	0.9	-	19
	SSA-1	0.66	0.32			1.737	0	0.895	7.843	19.01
						1.737	0.354	0.859	0	19.80
	SSA-2	0.676	0.304			1.780	0	0.852	8.236	18.50
						1.780	0.363	0.816	0	19.32
	exact	0.676	0.304			1.780	0.363	0.756	0	19.32
TpAT-tFFO in mCBP	original	0.02	0.82	6.536	2.262	0.11	0.20	5.3	-	120
	SSA-1	0.02	0.82			0.131	0	6.405	3.694	94.65
						0.131	0.249	6.380	0	95.02
	SSA-2	0.023	0.817			0.149	0	6.387	3.705	82.84
						0.149	0.284	6.358	0	83.21
	exact	0.023	0.817			0.149	0.284	5.549	0	83.21
Br-3PXZ-XO in toluene	original	0.033	0.42	20.00	20.41	0.68	-	19	120	260
	SSA-1	0.033	0.42			0.660	0	19.34	115.4	268.6
						0.660	7.970	18.54	0	280.1
	SSA-2	0.037	0.416			0.746	0	19.25	116.0	236.4
						0.746	9.005	18.35	0	247.9
	exact	0.037	0.416			0.746	9.005	16.08	0	247.9
DiKTa in toluene	original	0.25	0.01	19.61	0.435	4.9	140	0.75	-	0.46
	SSA-1	0.25	0.01			4.902	0	14.71	4.290	0.023
						4.902	139.5	0.754	-	0.452
	SSA-2	0.25	0.01			4.902	0	14.71	4.290	0.023
						4.902	139.5	0.754	-	0.452
	exact	0.25	0.01			4.902	139.5	0.754	0	0.452
MCz-TXT in mCBP	original	0.012[b]	0.908	107.3	13.33	1.3	-	94	-	1100
	SSA-1	0.012[b]	0.908			1.287	0	106.0	10.80	1021.0
						1.287	1.119	105.9	0	1022.2
	SSA-2	0.013[b]	0.907			1.287	0	105.8	10.81	933.2
						1.408	1.224	105.7	0	934.3
	exact	0.013[b]	0.907			1.408	1.224	96.51	0	934.3

a) using the PLQY before introduce the inert gas.

We also derived the "exact" rate equations for the TADF materials on the three-state model. In this model, Φ_{ISC} can be estimated without any other additional measurements other than emission spectra, transient emission decay, and PLQY. This method requires the estimation of Φ_{phos}, which can be obtained by spectral fitting or numerical analysis. However, there is difficult case because of the high accuracy of the equations. In this case, the equations allow to approximate $\Phi_{phos} \approx 0$, which can be applied to the data collected at temperatures where TADF is operational and is used in most of the literature reports. With the approximation of no phosphorescence contribution, the rate equations simplify and a consequence of this approximation within the model is that $\Phi_{nr}^{T} = 0$; i.e. the rate constants of radiative and non-radiative decay from T_1 are coupled. This method provides the most precise set of rate constants for TADF materials. Further, the exact equations reveal the presence of an important relationship on the photophysics; the singlet population decay is accelerated by the presence of a RISC process. By using either model reported here, we can derive the exact rate constants from reported values in the literature by analysing the data using the models of either Goushi-Masui or Dias, which are the ones most commonly used.

However, Ermolaev's rule approximates Φ_{nr}^{S} as zero (S_1 energy should have larger than 2.17 eV),[41,42] and it would be a problem to apply $\Phi_{nr}^{T} = 0$ especially in the case of low PLQY emitters. Therefore, we recommend to provide the average and maximum rate constants corrected by the exact solution for ISC rate (Table 2, Entry 5), if there is no specific reason, e.g., the material possessing extremely high PLQY. In this case, the maximum values of k_{RISC}, k_{nr}^{S}, and the minimum value of k_{ISC} correspond to the exact solution. Whatever the case, the four values of Φ_{PF}, Φ_{DE}, k_p, and k_d should be provided. We believe the equations provided here will enable the universalization of the kinetics analysis of TADF materials and so lead to a better understanding of their photophysics, and ultimately better materials.

Table 2. Summary of rate equations provided in this paper for three-state TADF system.

Entry	Equations	Comments
1	$k_r^S = k_p \Phi_{PF}$ $k_{nr}^S = k_p(1 - \Phi_{PF} - \Phi_{ISC})$ $k_{ISC} = k_p \Phi_{ISC}$ $k_r^T = k_d \frac{\Phi_{DE}(1 - R_{DE}^{DF})}{\Phi_{ISC}}$ $k_{nr}^T = k_d - (1 - \Phi_{ISC})k_{RISC} - k_r^T$ $k_{RISC} = \frac{k_d \Phi_{DE} R_{DE}^{DF}}{\Phi_{ISC}\Phi_{PF}}$	Assumption: $k_r^S + k_{nr}^S + k_{ISC} \gg k_{RISC}$ to approximate $k_p \approx k^S$ and apply steady state approximation. Requirement to obtain all rate constants k_{ISC} estimation or assuming $k_{nr}^S = 0$ or $k_{nr}^T = 0$ R_{DE}^{DF} estimation or approximate $R_{DE}^{DF} \approx 1$ $\Phi_r^S = \Phi_{PF} = \frac{k_d(A_p + A_d)}{A_p k_d + A_d k_p}\Phi_{PLQY}$ $\Phi_{DE} = \frac{A_d(k_p - k_d)}{A_p k_d + A_d k_p}\Phi_{PLQY}$
2	$k_r^S = k_p \Phi_{PF}$ $k_{nr}^{S\ Max} = k_p\left(1 - \Phi_{PF} - \frac{\Phi_{DF}}{\Phi_{PLQY}}\right)$ $k_{ISC}^{Ave.} = \frac{k_p}{2} \cdot \frac{\Phi_{PLQY}(1 - \Phi_{PF}) + \Phi_{DF} \pm \Phi_{PF}(1 - \Phi_{PLQY})}{\Phi_{PLQY}}$ $k_{nr}^{T\ Max} = k_d\left(1 - \frac{\Phi_{DF}}{1 - \Phi_{PF}}\right)$ $k_{RISC}^{Ave.} = \frac{k_d}{2} \cdot \frac{\Phi_{PLQY}(1 - \Phi_{PF}) + \Phi_{DF} \pm \Phi_{PF}(1 - \Phi_{PLQY})}{\Phi_{PF}(1 - \Phi_{PF})}$	Based on Entry 1. Assumption: $k_r^S + k_{nr}^S + k_{ISC} \gg k_{RISC}$ to approximate $k_p \approx k^S$ and apply steady state approximation. Approximation: $R_{DE}^{DF} \approx 1$ (or when $R_{DE}^{DF} = 1$) $\Phi_r^S = \Phi_{PF} = \frac{k_d(A_p + A_d)}{A_p k_d + A_d k_p}\Phi_{PLQY}$ $\Phi_{DF} = \frac{A_d(k_p - k_d)}{A_p k_d + A_d k_p}\Phi_{PLQY}$

3	$k_r^S = k_p \Phi_{PF}$ $k_{nr}^S = k^S - k_r^S - k_{ISC}$ $k_{ISC} = \frac{-b - \sqrt{b^2 - 4ac}}{2a}$ $k_{RISC} = \frac{(k_p - k^S)(k^S - k_d)}{k_{ISC}}$ $k_r^T = \frac{k_p k_d \Phi_{DE}(1 - R_{DE}^{DF})}{k_{ISC} + k_p - k^S}$ $k_{nr}^T = k_p + k_d - k^S - k_{RISC} - k_r^T$ $k^S = \frac{-1 + i\sqrt{3}}{2} \times \sqrt[3]{-g + \sqrt{g^2 + h^3}} + \frac{-1 - i\sqrt{3}}{2} \times \sqrt[3]{-g - \sqrt{g^2 + h^3}} - \frac{1}{3}d$	No assumption (require numerical analysis) $\Phi_{PF} = \frac{k_d(A_p + A_d)}{A_p k_d + A_d k_p} \Phi_{PLQY}$ $\Phi_{DE} = \frac{A_d(k_p - k_d)}{A_p k_d + A_d k_p} \Phi_{PLQY}$ $\begin{cases} a = \frac{\Phi_{DE}}{\Phi_{PF}} k_d R_{DE}^{DF} - k_p + k^S \\ b = (k_p - k^S)(k^S - k_p - k_d) - a k^S \\ c = (k_p - k^S)^2 (k^S - k_d) \end{cases}$ $\begin{cases} d = -\left[k_{ISC} + 3k_p + k_d\left(1 - \frac{\Phi_{DE}}{\Phi_{PF}}\right)\right] \\ e = k_{ISC} k_d \left[1 - \frac{\Phi_{DE}}{\Phi_{PF}}(2 - R_{DE}^{DF})\right] - k_p(3k_p + 2d) - {k_d}^2 \frac{\Phi_{DE}}{\Phi_{PF}} \\ f = -(k_{ISC} + k_p)(k_p + k_d)\left(k_p - k_d \frac{\Phi_{DE}}{\Phi_{PF}}\right) \end{cases}$ $\begin{cases} g = \frac{27f + 2d^3 - 9de}{54} \\ h = \frac{3e - d^2}{9} \end{cases}$
4	$k_r^S = k_p \Phi_{PF}$ $k_{nr}^S = k_p \frac{\Phi_{PF}}{\Phi_{PLQY}}(1 - \Phi_{PLQY})$ $k_{ISC} = k_p \frac{\Phi_{DF}}{\Phi_{PLQY}} - k_d \frac{\Phi_{DF}}{\Phi_{PF}}$ $k_{RISC} = k_d \frac{\Phi_{PLQY}}{\Phi_{PF}}$ $k_{nr}^T = 0$	Based on Entry 3. Approximation: $R_{DE}^{DF} \approx 1$ (or when $R_{DE}^{DF} = 1$) $\Phi_{PF} = \frac{k_d(A_p + A_d)}{A_p k_d + A_d k_p} \Phi_{PLQY}$ $\Phi_{DF} = \frac{A_d(k_p - k_d)}{A_p k_d + A_d k_p} \Phi_{PLQY}$
5	$k_r^S = k_p \Phi_{PF}$ $k_{nr}^{S\ Max} = k_p \frac{\Phi_{PF}}{\Phi_{PLQY}}(1 - \Phi_{PLQY})$ $k_{ISC}^{Ave.} = \frac{[k_p(1 - \Phi_{PF}) - k_d \Phi_{DF}]\Phi_{PLQY} + k_p \Phi_{PF} \Phi_{DF} \pm [k_p \Phi_{PF}{}^2 (1 - \Phi_{PLQY}) + k_d \Phi_{DF} \Phi_{PLQY}]}{2\Phi_{PF} \Phi_{PLQY}}$ $k_{nr}^{T\ Max} = k_d\left(1 - \frac{\Phi_{DF}}{1 - \Phi_{PF}}\right)$ $k_{RISC}^{Ave.} = \frac{k_d}{2} \cdot \frac{\Phi_{PLQY}(1 - \Phi_{PF}) + \Phi_{DF} \pm \Phi_{PF}(1 - \Phi_{PLQY})}{\Phi_{PF}(1 - \Phi_{PF})}$	Combination of Entries 2 and 4. Approximation: $R_{DE}^{DF} \approx 1$ (or when $R_{DE}^{DF} = 1$) $\Phi_{PF} = \frac{k_d(A_p + A_d)}{A_p k_d + A_d k_p} \Phi_{PLQY}$ $\Phi_{DF} = \frac{A_d(k_p - k_d)}{A_p k_d + A_d k_p} \Phi_{PLQY}$ $k_{nr}^{S\ Max}$, k_{ISC}^{Min} and k_{RISC}^{Max} are the same values with Entry 4.

ASSOCIATED CONTENT

Supporting information: Typical estimation methods in literature for k_{RISC} and k_{ISC} were summarized as Table S1 and S2, respectively. The several conversion equations from reported to corrected ones were provided. The validity of the approximation of $k^S \approx k_p$ by assuming $k^S \gg k_{RISC}$ were explained. The relationships of efficiencies between element and overall ones were provided. Several equations for derivation omitted in main text were provided. The detail of exciton distribution is explained. The derivation of rate equations standing on four-state photophysics were demonstrated with the minimum assumptions which related to El-Sayed's and Kasha's rules.
An excel spreadsheet for analysis is available on ChemRxiv; https://doi.org/10.26434/chemrxiv.14178113.

AUTHOR INFORMATION

Author Contributions

The manuscript was written through contributions of all authors.

Notes

The authors declare no competing financial interest.

ACKNOWLEDGMENT

Research at Kyushu, Kyoto and St Andrews Universities was supported by EPSRC and JSPS Core to Core grants (JSPS Core-to-core Program; EPSRC grant number EP/R035164/1). We are also grateful for financial support from the Program for Building Regional Innovation Ecosystems of the Ministry of Education, Culture, Sports, Science and Technology, Japan, JST ERATO Grant JPMJER1305, JSPS KAKENHI JP20H05840, and Kyulux Inc.

REFERENCES

(1) Wong, M. Y.; Zysman-Colman, E. Purely organic thermally activated delayed fluorescence (TADF) materials for organic light-emitting diodes (OLEDs). *Adv. Mater.* **2017**, *29*, 1605444.

(2) Yang, Z.; Mao, Z.; Xie, Z.; Zhang, Y.; Liu, S.; Zhao, J.; Xu, J.; Chi, Z.; Aldredb, M. P. Recent advances in organic thermally activated delayed fluorescence materials. *Chem. Soc. Rev.* **2017**, *46*, 915–1016.

(3) Liu, Y.; Li, C.; Ren, Z.; Yan, S.; Bryce, M. R. All-organic thermally activated delayed fluorescence materials for organic light-emitting diodes. *Nat. Rev. Mater.* **2018**, *3*, 18020.

(4) Bui, T.-T.; Goubard, F.; Ibrahim-Ouali, M.; Gigmes, D.; Dumur, F. Recent advances on organic blue thermally activated delayed fluorescence (TADF) emitters for organic light-emitting diodes (OLEDs). *Beilstein J. Org. Chem.* **2018**, *14*, 282–308.

(5) Kirchhoff, J. R.; Gamache Jr.; R. E.; Blaskie, M. W.; Paggio, A. A. D.; Lengel, R. K.; McMillin D. R. Temperature dependence of luminescence from $Cu(NN)_2^+$ systems in fluid solution. Evidence for the participation of two excited states. *Inorg. Chem.* **1983**, *22*, 2380–2384.

(6) Zhang, Q.; Li, B.; Huang, S.; Nomura, H.; Tanaka, H.; Adachi, C. Efficient blue organic light-emitting diodes employing thermally activated delayed fluorescence. *Nat. Photonics* **2012**, *8*, 326–332.

(7) Goushi, K.; Yoshida, K.; Sato, K.; Adachi C. Organic light-emitting diodes employing efficient reverse intersystem crossing for triplet-to-singlet state conversion. *Nat. Photonics* **2012**, *6*, 253–258.

(8) Masui, K.; Nakanotani, H.; Adachi, C. Analysis of exciton annihilation in high-efficiency sky-blue organic light-emitting diodes with thermally activated delayed fluorescence. *Org. Electron.* **2013**, *14*, 2721–2726.

(9) Kaji, H.; Suzuki, H.; Fukushima, T.; Shizu, K.; Suzuki. K.; Kubo, S.; Komino, T.; Oiwa, H.; Suzuki, F.; Wakamiya, A. et al. Purely organic electroluminescent material realizing 100% conversion from electricity to light. *Nat. Commun.* **2015**, *6*, 8476.

(10) Pan, K.-C.; Li, S.-W.; Ho, Y.-Y.; Shiu, Y.-J.; Tsai, W.-L.; Jiao, M.; Lee, W.-K.; Wu, C.-C.; Chung, C.-L.; Chatterjee, T. et al. Efficient and tunable thermally activated delayed fluorescence emitters having orientation-adjustable CN-substituted pyridine and pyrimidine acceptor units. *Adv. Funct. Mater.* **2016**, *26*, 7560–7571.

(11) Dias, F.; Penfold, T. J.; Monkman A. P. Photophysics of thermally activated delayed fluorescence molecules. *Methods Appl. Fluoresc.* **2017**, *5*, 012001.

(12) Wada, Y.; Nakagawa, H.; Matsumoto, S.; Wakisaka, Y.; Kaji, H. Organic light emitters exhibiting very fast reverse intersystem crossing. *Nat. Photonics* **2020**, *14*, 643–649.

(13) Hasse, N.; Danos, A.; Pflumm, C.; Morherr, A.; Stachelek, P.; Mekic, A.; Bütting, W.; Monkman A. P. Kinetic Modeling of transient photoluminescence from thermally activated delayed fluorescence. *J. Phys. Chem. C* **2018**, *122*, 29173–29179.

(14) Yurash, B.; Nakanotani, H.; Olivier, Y.; Beljonne, D.; Adachi, C.; Nguyen T.-Q. Photoluminescence Quenching probes spin conversion and exciton dynamics in thermally activated delayed fluorescence materials. *Adv. Mater.* **2019**, *31*, 1804490.

(15) Vázquez, R. J.; Yun, J. H.; Muthike, A. K.; Howell, M.; Kim, H.; Madu, I. K.; Kim, T.; Zimmerman, P.; Lee, J. Y.; Goodson III, T. New direct approach for determining the reverse intersystem crossing rate in organic thermally activated delayed fluorescent (TADF) emitters. *J. Am. Chem. Soc.* **2020**, *142*, 8074–8079.

(16) Scott, D. R.; Maltenieks, O. Experimental method for determining the intersystem crossing rate constant from lowest excited singlet to lowest triplet state. *J. Phys. Chem.* **1968**, *72*, 3354–3356.

(17) Carmichael, I.; Hug, G. L. Triplet-triplet absorption spectra of organic molecules in condensed phase. *J. Phys. Chem. Ref. Data* **1986**, *15*, 1–250.

(18) Berberan-Santos, M. N.; Garcia, J. M. M. Unusually strong delayed fluorescence of C_{70}. *J. Am. Chem. Soc.* **1996**, *118*, 9391–9394.

(19) Baleizão, C.; Berberan-Santos, M. N. Thermally activated delayed fluorescence as a cycling process between excited singlet and triplet states: Application to the fullerenes. *J. Chem. Phys.* **2007**, *126*, 204510.

(20) Kobayashi, T.; Kawate, D.; Niwa, A.; Nagase, T.; Goushi, K.; Adachi, C.; Naito, H. Intersystem crossing rate in thermally activated delayed fluorescence emitters. *Phys. Status Solidi A* **2020**, *217*, 1900616.

(21) Niwa, A.; Takaki, K.; Kobayashi, T.; Nagase, T.; Goushi, K.; Adachi, C.; Naito, H. Photoluminescence in a Thermally activated delayed fluorescence emitter for organic light-emitting diodes. *J. Imaging Soc. Jpn.* **2016**, *55*, 143–148.

(22) Kobayashi, T.; Niwa, A.; Haseyama, S.; Takaki, K.; Nagase, T.; Goushi, K.; Adachi, C. and Naito, H. Emission properties of thermally activated delayed fluorescence emitters: analysis based on a four-level model considering a higher triplet excited state. *J. Photon. Energy* **2018**, *8*, 032104.

(23) Serevičius, T.; Skaisgiris, R.; Kreiza, G.; Dodonova, J.; Kazlauskas, K.; Orentas, E.; Tumkevičius, S.; Juršėnas, S. TADF Parameters in the Solid State: An Easy Way to Draw Wrong Conclusions. *J. Phys. Chem. A* **2021**, *125*, 1637–1641.

(24) Zhang, Q.; Kuwabara, H.; Potscavage, Jr.; W. J.; Huang, S.; Hatae, Y.; Shibata, T.; Adachi, C. Anthraquinone-Based Intramolecular Charge-Transfer Compounds: Computational Molecular Design, Thermally Activated Delayed Fluorescence, and Highly Efficient Red Electroluminescence. *J. Am. Chem. Soc.* **2014**, *136*, 18070–18081.

(25) Notsuka, N.; Nakanotani, H.; Noda, H.; Goushi, K.; Adachi, C. Observation of nonradiative deactivation behavior from singlet and triplet states of thermally activated delayed fluorescence emitters in solution. *J. Phys. Chem. Lett.* **2020**, *11*, 562–566.

(26) Etherington, M. K.; Gibson, J.; Higginbotham, H. F.; Penfold, T. J.; Monkman, A. P. Revealing the spin-vibronic coupling mechanism of thermally activated delayed fluorescence. *Nat. Commun.* **2016**, *7*, 13680.

(27) Kobayashi, T.; Niwa, A.; Takaki, K.; Haseyama, S.; Nagase, T.; Goushi, K.; Adachi, C.; Naito H. Contributions of a higher triplet excited state to the emission properties of a thermally activated delayed-fluorescence emitter. *Phys. Rev. Appl.* **2017**, *7*, 034002.

(28) Noda, H.; Chen, X.-K.; Nakanotani, H.; Hosokai, T.; Miyajima, M.; Notsuka, N.; Kashima, Y.; Brédas, J.-L.; Adachi, C. Critical role of intermediate electronic states for spin-flip processes in charge-transfer-type organic molecules with multiple donors and acceptors. *Nat. Mater.* **2019**, *18*, 1084–1090.

(29) Zysman-Colman. E. Molecular designs offer fast exciton conversion. *Nat. Photonics* **2020**, *14*, 593–594.

(30) Tsuchiya, Y.; Tsuji, K.; Inada, K.; Bencheikh, F.; Geng, Y.; Kwak, H. S.; Mustard, T. J. L.; Halls, M. D.; Nakanotani, H.; Adachi, C. Molecular design based on donor-weak donor scaffold for blue thermally-activated delayed fluorescence designed by combinatorial DFT calculations. *Front. Chem.* **2020**, *8*, 403.

(31) El-Sayed, M. A. Spin-orbit coupling and the radiationless processes in nitrogen heterocyclics. *J. Chem. Phys.* **1963**, *38*, 2834–2838.

(32) Kasha, M. Characterization of electronic transitions in complex molecules. *Discuss. Faraday Soc.* **1950**, *9*, 14–19.

(33) Noda, H.; Nakanotani, H.; Adachi, C. Excited state engineering for efficient reverse intersystem crossing. *Sci. Adv.* **2018**, *4*, eaa06910.

(34) Cui, L.-S.; Gillett, A. J.; Zhang, S.-F.; Ye, H.; Liu, Y.; Chen, X.-K.; Lin, Z.-S.; Evans, E. W.; Myers, W. K.; Ronson, T. K. et al. Fast spin-flip enables efficient and stable organic electroluminescence from charge-transfer states. *Nat. Photonics* **2020**, *14*, 636–642.

(35) Mamada, M.; Inada, K.; Komino, T.; Potscavage Jr.; W. J.; Nakanotani, H.; Adachi. C. Highly Efficient Thermally Activated Delayed Fluorescence from an Excited-State Intramolecular Proton Transfer System. *ACS Cent. Sci.* **2017**, *3*, 769–777.

(36) Kondo, Y.; Yoshiura, K.; Kitera, S.; Nishi, H.; Oda, S.; Gotoh, H.; Sasada, Y.; Yanai, M.; Hatakeyama, T. Narrowband deep-blue organic light-emitting diode featuring an organoboron-based emitter. *Nat. Photonics* **2019**, *13*, 678–682.

(37) Kim, J.-U.; Park, I.-S.; Chan. C.-Y.; Tanaka, M.; Tsuchiya, Y.; Nakanotani. H.; Adachi, C. Nanosecond-time-scale delayed fluorescence molecule for deep-blue OLEDs with small efficiency rolloff. *Nat. Commun.* **2020**, *11*, 1765.

(38) Aizawa, N.; Harabuchi, Y.; Maeda, S.; Pu, Y.-J. Kinetic prediction of reverse intersystem crossing in organic donor–acceptor molecules. *Nat. Commun.* **2020**, *11*, 3909.

(39) Hall, D.; Suresh, S. M.; dos Santos, P. L.; Duda, E.; Bagnich, S.; Pershin, A.; Rajamalli, P.; Cordes, D. B.; Slawin, A. M. Z.; Beljonne, D. et al. Improving Processability and Efficiency of Resonant TADF Emitters: A Design Strategy. *Adv. Opt. Mater.* **2020**, *8*, 1901627.

(40) Aizawa, N.; Matsumoto, A.; Yasuda, T.; Thermal equilibration between singlet and triplet excited states in organic fluorophore for submicrosecond delayed fluorescence. *Sci. Adv.* **2021**, *7*, eabe5769.

(41) Turro, N. J.; Ramamurthy, J.; Scaiano, J. C. *Principles of Molecular Photochemistry: An Introduction*; University Science Books: Sausalito, CA, USA, 2009.

(42) Ermolaev V. L.; Energy transfer in organic systems involving the triplet state III. Rigid solutions and crystals. *Phys.-Usp.* **1963**, *6*, 333–358.

ToC Graphics

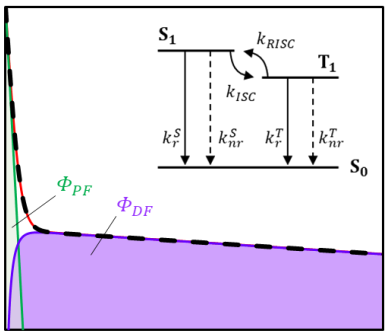

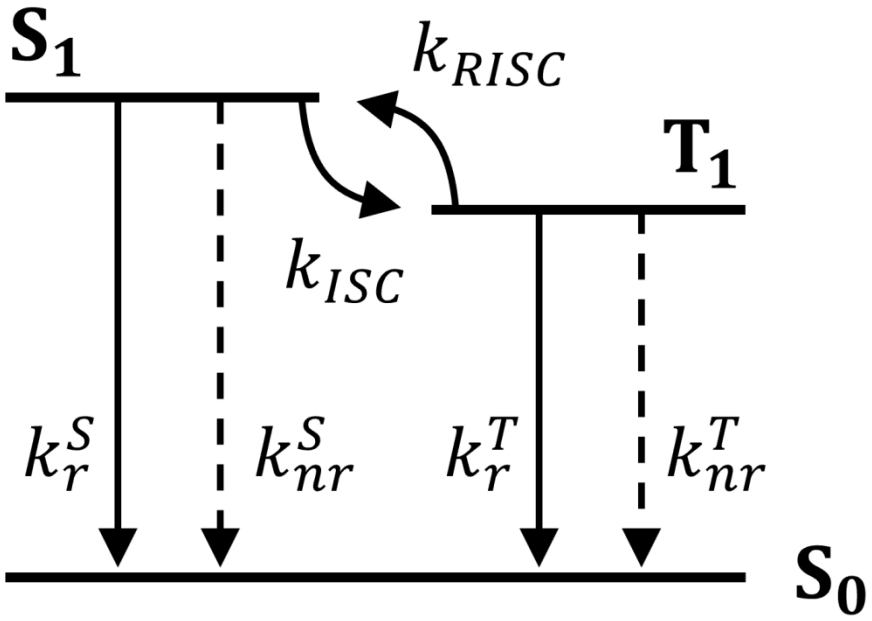

The scheme of photophysical process for three-state system.

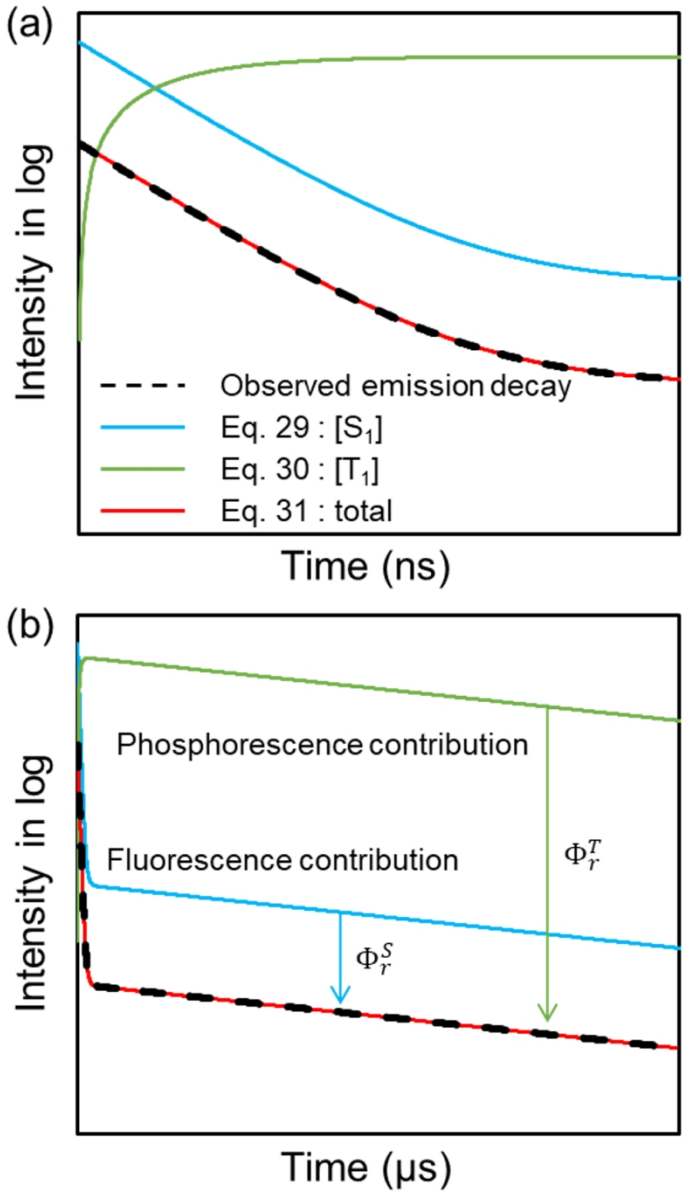

Emission decay curve and theoretical curves of Eqs. 29-31 within nanosecond time range (a) and microsecond time range (b). The difference of total emission and exciton population decays is related to the fluorescence and phosphorescence contributions depending on emitting ratio of each exciton.

359x611mm (72 x 72 DPI)

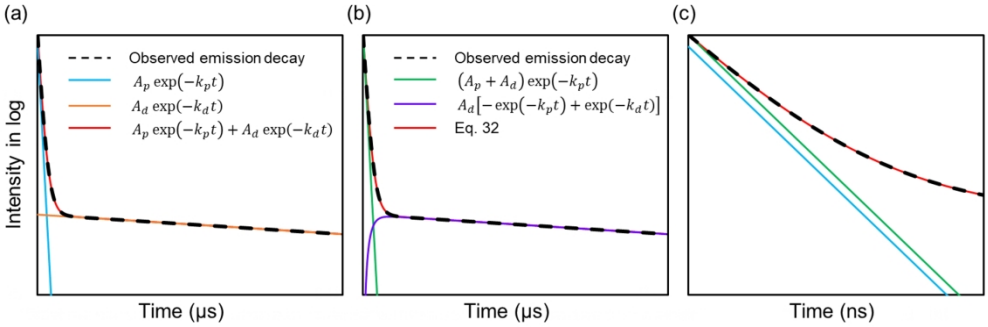

(a) Emission decay curve and biexponential fitting curves which are employed to estimate the prompt and delayed emission efficiency in gen-eral. (b) Corrected prompt and delayed component curves to provide exact emission efficiencies. (c) Closeup within nano second range to recognise difference of prompt components for general and corrected estimation method.

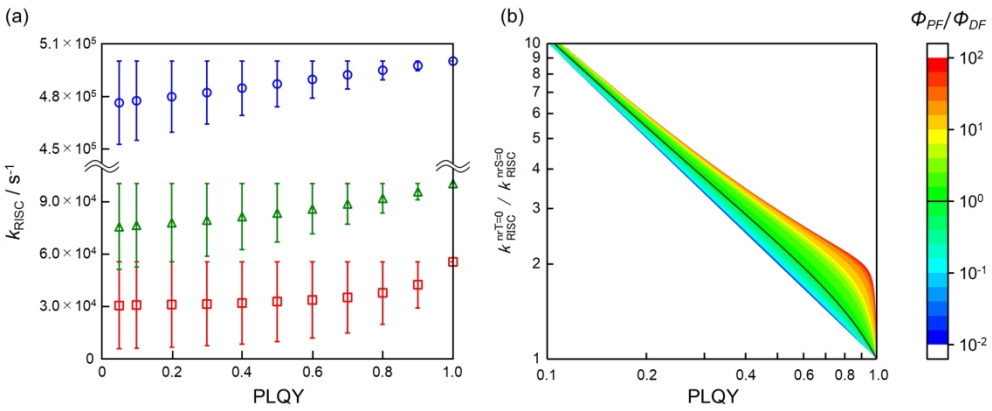

(a) Plot of k_RISC^(Avg.) for the delayed emission ratio to PLQY; blue circle, Φ_PF:Φ_DF=0.1:0.9; green triangle, Φ_PF:Φ_DF=0.5:0.5; red square, Φ_PF:Φ_DF=0.9:0.1; 1/k_p , 20 ns; 1/k_d , 20 μs; plot was generated using Eq. 61. (b) Ratio of RISC rate constant between assuming k_nr^S=0 and k_nr^T=0 for each PLQY with color properties indicating the ratio of Φ_PF and Φ_DF; solid black line, Φ_PF:Φ_DF=1; plot was generated by using Eq. 61.